Early functional mismatch between breast cancer cells and their tumour microenvironment suppresses long term growth

Anna Perdrix Rosell[1,2,3], Oscar Maiques[2,3], Probir Chakravarty[4], Luigi Ombrato[1,5], Victoria Sanz-Moreno[2,3#] & Ilaria Malanchi[1#]

[1]Tumour Host Interaction Laboratory, The Francis Crick Institute, 1 Midland Road,NW1 1AT London, UK.

[2]Sanz-Moreno Lab, Centre for Tumour Microenvironment, Barts Cancer Institute, Queen Mary University of London, Charterhouse Square, London EC1M 6BQ, UK.

[3]Randall Division of Cell and Molecular Biophysics, King's College London, New Hunt's House, Guy's Campus, London SE1 1UL, UK.

[4]Bioinformatics and Biostatistics Unit, The Francis Crick Institute, 1 Midland Road,NW1 1AT London, UK.

[5]Current address: Ombrato Lab, Centre for Tumour Microenvironment, Barts Cancer Institute, Queen Mary University of London, Charterhouse Square, London EC1M 6BQ, UK.

correspondence to v.sanz-moreno@qmul.ac.uk and Ilaria.malanchi@crick.ac.uk.

The authors declare no potential conflicts of interest.

Running Title: Early tumour microenvironment determines long term growth

Abstract

Cancer cells thrive embedded in a fine-tuned cellular and extracellular environment or tumour microenvironment (TME). There is a general understanding of a co-evolution between cancer cells and their surrounding TME, pointing at a functional connection between cancer cells characteristics and the perturbations induced in their surrounding tissue. However, whether this functional connection needs to be set from the start or if aggressive cancer cells can always be dominating their microenvironment has never been formally proven with a dedicated experimental setting where malignant cells can be challenged to grow in a different TME from the one they would naturally create. Here we generated an experimental setting where we transiently perturb the secretory profile of aggressive breast cancer cells without affecting their intrinsic growth ability. This led to the initial establishment of an atypical TME. Interestingly, even if initially tumours are formed, this atypical TME evolves to impair long term *in vivo* cancer growth. Using a combination of in vivo transcriptomics, protein arrays and in vitro co-cultures, we found that the atypical TME culminates in the infiltration of macrophages with STAT1^{high} activity. These macrophages show strong anti-tumoural functions which reduce

long-term tumour growth, despite lacking canonical M1 markers. Importantly, gene signatures of the mesenchymal compartment of the TME, as well as the anti-tumoural macrophages show striking prognostic power-correlating with less aggressive human breast cancers.

Introduction

Cancer cells have the ability to generate a special cellular and extracellular environment to support their growth, which is collectively named tumour microenvironment (TME). This local ecosystem comprises an acellular part, characterized by a dense network of extracellular matrix (ECM) proteins, as well as a variety of cellular components (1). For instance, cancer-associated fibroblasts (CAFs) are one of the more dominant components of the TME and master secretors of ECM proteins and play a key role in tumour progression, tumour invasion and metastasis (2-4). Moreover, a multifaceted array of innate immune-cells, such as monocytes, macrophages and neutrophils, promotes tumorigenesis and metastatic dissemination (5-7). However, macrophages, which have a pivotal role in orchestrating cancer related inflammation, can have a dual supportive or inhibitory role in the cancer context (8). Importantly, the type of intra-tumoral immune infiltration in different cancer contexts is determined by the properties of the TME, for instance CAFs can contribute to the recruitment of immunosuppressive cells: tumour-associated macrophages (TAMs) or regulatory T lymphocytes (9).

An essential aspect of aggressive cancer cells is their ability to change their cytoskeleton to grow, invade, metastasize and evade the immune system. A key regulator of the cytoskeleton is Rho-associated coiled-coil containing protein kinase (ROCK) which increases Myosin II activity (10) and cancer invasion. Aside from its well described role in metastasis (11), ROCK has been shown to promote intrinsic tumorigenic ability of tumours of mesenchymal origin such as melanoma (12-14). Importantly, the tumorigenic potential of cancer cells is coupled to their extrinsic ability to promote a tumour supporting TME (15). Indeed, the fact that more contractile melanoma cells have a dinstinct secretory profile which alters the properties of TME components (1,16), advocate for the idea that the activation of pathways supporting cancer cells tumorigenic potential is directly linked to their ability to create their optimal cellular ecosystem within that tissue.

The fact that different tumour types have different cellular composition in their TME (17), rises the intriguing possibility that a specific match between the intrinsic characteristics of cancer cells and the kind of TME established is required to support their growth. In this view, it would be critical for a tumour to achieve a co-ordinated and fine-tuned TME establishment. In this case, a variation in the initial cancer cell-TME set up could result in an enduring mismatch that will ultimately impair tumour progression. However, whether changes in the initial TME typical of a particular cancer cell type, can act as dominant limiting factor for long-term tumour growth, or whether highly tumorigenic cells are able to re-adjust their TME

in order to proficiently grow, is not known. This is due to challenging experimental set up required to address this question.

Here, we present an experimental setting where the secretion profile of the aggressive murine breast cancer 4T1 cells is perturbed by transitory inhibition of ROCK-Myosin II signalling either via the pre-treatment with a specific inhibitor or the use of inducible shRNA. Crucially, this does not influence 4T1 growth ability in vitro, but triggers a transient perturbation in the release of extrinsic factors that will initiate a different TME compared to the one they would normally create when grafted in the fat pad. Even when, at early stages of tumour growth, cancer cells recover their initial properties, we found that such TME limits their long-term cancer growth. This is due to the recruitment of a different stroma and the generation of anti-cancer macrophages. Therefore, this work represents a direct experimental evidence that the creation of an early optimal microenvironment is a dominant factor in the cascade of events determining long-lasting cancer growth and describe the signature of unusual anti-cancer macrophages which maintain M2 markers.

Results

Experimental uncoupling of cancer cells intrinsic growth potential and ability to activate stromal cells *in vitro*.

To assess whether a variation in the initial cancer cell-TME set up could result in an enduring mismatch that will ultimately impair tumour progression, we sought a way to reversibly interfere exclusively with extrinsic features of cancer cells without negatively influencing their intrinsic tumorigenic potential. This should alter the initial interaction with their local environment and in turn generate a different TME. However, the cancer cells need to quicky regain their initial characteristics, to create the situation of a mismatch between the cancer cell type and its typical microenvironment *in vivo*.

Melanoma cells have been previously shown to have altered secretome upon treatment with the highly specific ROCK inhibitor GSK269962 (from now on named GSKi) (12,16). However, in melanoma, this signalling is generally essential for their growth potential. Conversely, human breast cancer lines show a variable level of intrinsic susceptibility to GSKi, and a substantial number of cell lines do not show an intrinsic response to the drug when treated *in vitro* for 3 days (Figure 1A). If alterations in the secretome of breast cancer cells is maintained, this treatment could potentially uncouple extrinsic features from intrinsic requirements. We therefore used GSKi to select a murine cell line able to maintain intrinsic growth capacity upon GSK addition and test if this still affected their secretion pattern. Cells were acutely exposed to GSKi for 5 days and their growth in different conditions was assessed after treatment interruption (pGSKi or pre-treated) (Figure 1B). The lower levels of MLC2 phosphorylation (pMLC2) confirmed that inhibition was maintained for at least three days after stopping the treatment in the murine 4T1 breast cancer cell line (Figure 1C and D). While pGSKi in other cell line, the 4T07 breast cancer line, caused reduced long-term growth (Supplementary Figure 1A and B), we found that did not reduced 4T1 cell growth in different *in vitro* conditions. (Figure 1E-G and Supplementary Figure 1C and D). Importantly, during this period, less contractile 4T1 cells showed an alteration in various secreted factors found in the culture media (Figure 1H and I). To assess the functional relevance of this perturbation in the secretome, we used classical fibroblast activation assays *in vitro*. After confirming the absence of GSKi in culture media of pre-treated cells by mass spectrometry (Supplementary Figure 1E), we found that both control and pGSKi-4T1 cancer cells similarly influence fibroblast proliferation *in vitro*. Nonetheless, these fibroblasts displayed different functional characteristics such as morphology, extracellular matrix contraction and migration abilities (Supplementary Figure 1F-J). These data indicate that, in principle pGSKi-4T1 cancer cells

124 altered normal fibroblasts' activation *in vitro*. As tumour associated fibroblasts are the most
125 abundant and a key cellular component of the stroma in breast cancer (18), this data suggest
126 that pre-treatment with GSKi could effectively uncouple intrinsic growth abilities and extrinsic
127 host activating functions in 4T1 cancer cells, creating the ideal setting to address our research
128 question.
129
130 **Early alterations in the TME causes long-term growth inhibition *in vivo***
131 Next, we tested the capacity of 4T1 cells pre-treated with GSKi (pGSKi-4T1) to form tumours
132 when implanted in the fat pad of syngeneic Balb/c mice (Figure 2A). We found that while the
133 initial phase of tumour establishment (8 days post-transplantation) was unaffected, the long-
134 term growth ability of pGSKi-4T1 cells was strongly compromised (from 14 days post-
135 transplantation) (Figure 2B and C). Importantly, at an early stage of tumour establishment-a
136 time point where tumour growth was unaltered, the overall levels of pMLC2, monitoring the
137 effect of the inhibitor, were nearly fully recovered from the GSKi pre-treatment, confirming its
138 transient effect in vivo (Figure 2D and Supplementary Figure 2A-C). This unaltered early
139 growth is in line with the unaffected intrinsic ability of cancer cell growth observed *in vitro* in
140 pGSKi-4T1 (Figure 1E-G and Supplementary Figure1A and B). The long-term reduction of
141 tumour growth resulting from GSK treatment was similarly achieved by specifically removing
142 its target effector MYL9/MYL12B (genes encoding Myosin Light Chain 2) with an inducible
143 shRNA (Supplementary Figure 2F-H). In this case, the effect in cancer cells was induced
144 transiently as the mice were maintained under doxycycline induction only for 5 days post-
145 transplantation. Similarly, to the results using GSKi pre-treatment, this resulted in an initial
146 unperturbed growth (day 10), follow by a growth reduction and a long-term growth suppression
147 (Supplementary Figure 2F-H).
148 Given that we have shown that pre-treated with GSKi altered the cancer-stromal interactions
149 in vitro and that pGSKi-4T1 tumours suffer a delay in growth after the effect of the inhibitor
150 has disappeared, we hypothesised that this delay could be due to the initial altered TME that
151 might be less fit to support long term tumour growth. To test this hypothesis, we isolated cells
152 from early-stage tumours, when tumour growth is not affected, and cancer cells have
153 recovered from GSKi effects (Figure 2E). For this experiment we used 4T1 cells which were
154 labelled by a extracellular domain of a human CD2 (hCD2) receptor. By magnetic cell sorting
155 (MACS), we isolated either CD2+ cancer cells (A) or, alternatively, the rest of the TME
156 depleted cells from the majority of cancer cells (B) (Figure 2F). By re-transplanting the isolated
157 cells in new recipient mice, we tested the ability of 4T1 cells from pGSKi-4T1 tumours to re-
158 establish secondary tumour growth alone or when maintained in the overwhelming presence

159 of the TME they have previously established (Figure 2F). In line with the fact that GSKi effects
160 was now cleared (Figure 2E and Supplementary Figure 2A-C), 4T1 cells from pGSKi-4T1
161 tumours show no delay in sustaining long term growth upon re-transplantation compared to
162 control cells (Figure 2G). Strikingly, when the same cancer cells were re-transplanted together
163 with the previously established TME, tumours still show a strong reduction of growth in
164 secondary recipient (Figure 2H). These results point at a dominant inhibitory effect of the TME
165 generated in pGSKi-4T1 tumours on cancer cells, which otherwise would possess an
166 unaltered growth capacity.
167
168 **Early differences in stromal cells in inhibitory TME**
169 We next analysed the TME cellular composition of tumours from control and pGSKi-4T1 cells
170 after cancer establishment. Early pGSKi-4T1 tumours showed an increase in αSMA+ stromal
171 cells, one of the dominant TME components already in control 4T1 tumours (Figure 3A and
172 B). To test if the characteristics of the stromal compartment were different in the inhibitory
173 TME, we isolated the general stromal compartment, depleted from immune-cells and
174 endothelial cells, of tumours from pGSKi-4T1 cells (Figure 3C) at the early time point, when
175 growth was unaltered. Deep RNA sequencing showed a different signature of stromal cells
176 from pGSKi-4T1 compared to stromal cells isolated from control tumours (Figure 3D and E).
177 However, when we functionally tested these alternatively activated stromal cells for their ability
178 to support cancer cell growth, no difference was detected neither in 3D co-culture system nor
179 in co-injection assay *in vivo* (Supplementary Figure 3A-D). We had previously observed that
180 fibroblast activation *in vitro* was perturbed in pGSKi-4T1 cells (Supplementary Figure 1F-J)
181 and similarly, we observed no difference in tumour growth also when co-injecting *in vitro*
182 activated fibroblasts (Supplementary Figure 3E and F). This suggests that these differently
183 activated stromal cells do not show anti-tumour effect per se, but they reflect the early
184 generation of an altered TME initiated by pGSKi-4T1 cells.
185 When analysing the features of the alternative TME captured by its stromal signature, we
186 found that extracellular matrix (ECM) regulation and integrin signalling were upregulated
187 (Figure 3E) pointing at changes within the non-cellular ECM compartments of the TME. We
188 could indeed validate this observation by detecting an increase in matrix density and Collagen
189 IV staining in the pGSKi-4T1 tumours compared to control (Supplementary Figure 3G and H).
190 Importantly, the stromal signature found in tumours generated by pGSKi-4T1 cells which show
191 reduced activation, Low Active (LA)-TME signature, showed strong prognostic power to
192 identify human breast cancer patients with better survival in TCGA database (Figure 3F-H).
193 This indicates that this lower level of typically activated pathways in the stromal signature

194 characterized less aggressive human breast cancers. Indeed, this LA-TME signature shows
195 downregulation of pathways key for CAF function (Figure 3E), suggestive of a failure to
196 establish the suitable pro-tumoral activity needed in the TME of aggressive and fast growing
197 tumours.
198
199 **Inhibitory TMEs contain different immuno-infiltrates**
200 Bioinformatic analysis showed that a major difference in the enriched pathways in pGSKi-4T1
201 tumour's stroma was lower activation of inflammatory signalling pathways/chemokines and
202 cytokine release, suggesting that broader alterations could be triggered within the
203 inflammatory TME compartment (Figure 3E). Consistently, when the immune-cell composition
204 of tumours was analysed by FACS, we found significant differences in control or pGSKi-4T1
205 tumours specifically at later time points (Figure 4A-H). Data showed a decrease in cells from
206 the lymphoid lineage in favour of an increase in myeloid cells.
207 To test if a decrease in tumour infiltrating lymphocytes could contribute to the delay in tumour
208 growth, control or pGSKi-4T1 cells were transplanted in immune-compromised RAG1-/- mice,
209 lacking B and T lymphocytes. Similar delays in the growth of pGSKi-4T1 tumours were
210 observed, excluding an involvement of the adaptive immune system to limit tumour growth
211 (Figure 4I and J).
212 Macrophages are known to possess both pro- and anti-tumorigenic functions (19), therefore
213 we tested if different macrophage polarizationcould be detected in pGSKi-4T1 tumours.
214 Tumour associated macrophages (TAM) showed no difference in canonical markers that have
215 been previously associated to pro- or anti-cancer activities (Supplementary Figure 4A and B).
216 Accordingly, when analysing the immune-infiltrates in the TCGA human breast cancers
217 classified according to the pGSKi-4T1 tumours stromal signature, there was no difference in
218 M1 or M2 macrophages (Supplementary Figure 4C). Collectively, these data show that the
219 change in lymphocyte infiltration status of the pGSKi-4T1 TME it is not responsible for the
220 reduced growth. Surprisingly, the macrophages infiltrating these tumours still express
221 classical pro-tumorigenic markers.
222
223 **Inhibitory TMEs harbour macrophages with non-canonical anti-cancer activity**
224 We next aimed to determine if, despite showing canonical TAM markers, macrophages in
225 pGSKi-4T1 tumours, harbour different characteristics. To do this, we generated a gene
226 expression signature of F4/80 macrophages isolated from control or pGSKi-4T1 tumours
227 (Figure 5A). Striking differences were detected at the gene expression level (Figure 5B and
228 C). Interestingly, the emergence of a distinct signature was detected 8 days post-

229 transplantation and was consolidated at later time points, when tumour growth was
230 significantly reduced (Figure 5B and C).
231 Analysis of the macrophage signature from the two types of tumours using GSEA revealed an
232 increase in anti-tumour inflammation Interferon gamma (INFγ) signalling and a decrease in
233 pro-tumour inflammation NFκB signalling in pGSKi-4T1 tumour derived macrophages (Figure
234 5D), pointing to an anti-tumour function. Importantly, when we analysed the conditioned media
235 of stromal cells isolated from pGSKi-4T1 tumours at 14 days, we detected a dramatic decrease
236 in specific secreted factors cytokines compared to control tumours (Supplementary Figure
237 5A). Particularly, at this tumour stage, network enrichment analysis of the secretome
238 supported the overall decrease in NFκB signalling within stromal cells (Supplementary Figure
239 5B), which was previously reported to be critical for CAF-mediated enhancement of tumour
240 promoting inflammation (20). The activation of INFγ activity indicated by the signature of
241 infiltrating macrophages of pGSKi-4T1 tumours, was confirmed by a sharp increase in active
242 STAT1 nuclear staining in such macrophages at late time points (Figure 5E and F).
243 Consistently with a growth defect , similar pSTAT1+ macrophages were detected at the late
244 stage of tumours initiated by cells transiently affected by MYL9/12b knock down
245 (Supplementary Figure 2D-F and 5E). Interestingly, already at early stages, infiltrating
246 macrophages of pGSKi-4T1 tumours sowed increased pSTAT1 staining (Supplementary
247 Figure 5C). Moreover, as predicted by their signature, we also measured a reduction in nuclear
248 p65 (RelA component of the NFκB complex) in macrophages from pGSKi-4T1 tumours
249 (Supplementary Figure 5D), which results in an overall switch from NFκB to INFγ -STAT1
250 signalling activity (Figure 5G). We therefore hypothesise that macrophages in pGSKi-4T1
251 tumours undergo profound transcriptional re-programming that might compromise their pro-
252 tumorigenic potential without changing some key cell surface markers.
253 To assess the functional implications of the changes observed in macrophages, we tested
254 their direct interaction with cancer cells by using a 3D co-culture scaffold system. We used
255 primary breast tumour cells isolated from spontaneous Actin-GFP/MMTV-PyMT breast
256 tumours in the co-culture. Freshly isolated macrophages from either control or pGSKi-4T1
257 tumours showed no differential activity when co-cultured alone with cancer cells seeded on
258 3D scaffolds (Supplementary Figure 5F-H). However, when cancer cells were seeded together
259 with their cancer associated stromal cells, macrophages isolated from 14 days pGSKi-4T1
260 tumours showed a cancer inhibitory effect (Figure 5H and I). Similar results were observed in
261 2D culture conditions (Figure 5J, 5K). Fibroblasts supported the cancer cell killing activity of
262 macrophages isolated from pGSKi-4T1 tumours independently from their origin. when isolated
263 from pGSKi-4T1 tumours or control (DMSO) tumours (Figure 5K). These data suggest that

264 the anti-tumour polarization observed in macrophages from pGSKi-4T1 is progressively
265 established within the complex *in vivo* TME and it becomes a hardwired status.
266
267 **Non-canonical pGSKi-4T1 macrophages are responsible for limiting tumour growth.**
268 To test whether this non-canonical anti-tumour polarization of macrophages was acting to limit
269 cancer cell growth *in vivo*, we used clodronate to deplete macrophages from control or pGSKi-
270 4T1 cell transplants (Figure 6A). In line with the known pro-tumour activity of tumour infiltrating
271 macrophages in breast cancer (19), their depletion decreased the final size reached by control
272 tumours (Figure 6B). However, an opposite effect was shown in pGSKi-4T1, where their
273 depletion boosted overall tumour growth and rescued it to the level of control tumours (Figure
274 6C). This data highlighted that the alternative macrophage polarization we described, indeed
275 results in a switch from pro- to anti-tumour function.
276 We have shown in Figure 3 that the activated stroma from pGSKi-4T1 cells harbour a gene
277 signature (LA-TME signature) with prognostic value in human breast cancer. Similarly, we
278 generated the macrophages LA-TME signature using the downregulated genes in
279 macrophages from pGSKi-4T1 tumours. Strikingly, we found that the macrophage LA-TME
280 signature showed a similar power in predicting better survival of human breast cancer patients
281 (Figure 6D). Moreover, 43% of these human tumours additionally showed the alternative
282 stroma LA-TME signature, suggesting a similar overall reduction of activation in stromal cells
283 and macrophages genes in the tumour microenvironment can be found in human breast
284 cancers with better prognosis (Figure 6E). Most importantly, as no difference was found in
285 macrophage markers generally associated to anti-tumour phenotypes in breast tumours
286 (Supplementary Figure 4A-C), this data suggests the presence of a previously unappreciated
287 alternative type of anti-tumour macrophages, which correlates with better clinical outcome.
288 Overall, this study show that an initial deviation in the initial stage of cancer-host interaction
289 cause by a perturbation of the malignant cancer cells secretion, results in the long term
290 establishment of a suboptimal TME which becomes dominant in suppressing aggressive
291 tumour growth.
292

293 **Discussion**

294

295 In this work, we show that the initial TME typical of a particular cancer cell type, can act as
296 dominant limiting factor for long term tumour growth. To test this, we have generated an
297 experimental set-up which allows to interfere exclusively with the extrinsic features of an
298 aggressive cell line without negatively influencing its intrinsic growth potential. This change
299 induces an initial atypical interaction with the *in vivo* environment which is different from what
300 these cancer cells would induce. In turn, this generates an initial alternative TME. As the
301 nature of the perturbation induced in the cancer cells is temporary, they recover their initial
302 characteristics when embedded in this atypical microenvironment *in vivo.* By creating this
303 complex experimental strategy, we here formally show that a sub-optimal TME becomes
304 dominant in suppressing the growth of highly aggressive cancer cells. In this work, also show
305 that ROCK-Myosin II activation in this breast cancer cell line with basal characteristics control
306 their secretion activity and modulate the initial activation of host cells in vitro and in vivo without
307 altering their intrinsic growth potential. This is intriguing as cancer cells displaying high ROCK-
308 Myosin II activation, generally relay on this pathway for their intrinsic tumourigenicity (16), but
309 we identify a murine breast cancer cell line which represented an exception and where it
310 exclusively interferes with the secretion profile of the cells. Indeed, the aggressive murine 4T1
311 breast cancer maintained its highly proliferative activity in various vitro conditions upon ROCK-
312 Myosin II inhibition but showed a perturbed fibroblast activation ability. After identifying the
313 4T1 as a cell line where the intrinsic and extrinsic activity could be uncoupled using ROCK-
314 Myosin II inhibition, we used ROCK-signalling inhibitor (GSK269962A) (GSKi) pre-treatment
315 before transplanting cancer cells *in vivo* to only transiently perturbe their interactions with the
316 host environment. Even when the GSKi effect ceased and cancer cells recover ROCK-Myosin
317 II activity, are now less capable to sustained long-term growth. Secondary transplantation
318 experiments show that, while cancer cells recover their full in vivo tumourigenicity when
319 growing secondary tumours, is the TME generated by initially pre-treated GSKi 4T1 cells who
320 imposes a limitation for their growth.
321 Our data supports the fact that GSKi pre-treated cancer cells initiate an atypical TME
322 characterized by an increase early representation of SMA positive cells, which, similar to the
323 in vitro activated fibroblasts, show different characteristics and signature compare to the one
324 that unperturbed 4T1 would have generated. Secretome analysis on GSKi pre-treated 4T1
325 conditioned media revealed significant differences with control 4T1 media in the secretion of
326 20 cytokines (where LIF, WISP1, MMP9 and several others resulted downregulated in pGSKi),
327 some of which have been previously linked to CAF activation. For instance, cancer-derived

328 LIF was shown to promote CAF activation and pro-invasive phenotype via inducing
329 actomyosin contractility and ECM remodelling (21). In addition, WISP1 was found in the
330 metastatic niche and was required for breast cancer metastasis to the lung (22). Thus, it is
331 tempting to speculate that such a differential cocktail of factors could interfere with the pro-
332 tumorigenic stromal activation generally induced by 4T1 cells.
333 Strikingly, despite the transcriptomic analysis of stromal TME component from control or GSKi
334 pre-treated tumours shows an atypical gene-expression signature, they similarly supported
335 cancer cell growth *ex-vivo* and *in vivo*. This data suggests that in principle, they can support
336 cancer cell growth. Nonetheless, within the TME, this atypical stromal component is part of a
337 more complex environment, which ultimately results to be unfit to support aggressive tumour
338 growth. In particularly, we detected a reduced activation of inflammatory signalling NFkB,
339 which iscrucial for the establishment of pro-tumoral inflammation (20). This lack of activation
340 has the potential to have a broader impact on the immune compartment in the TME. Indeed,
341 when analysing the tumour infiltrates, we identified a reduction on lymphocytic cells (B and T-
342 cells, specifically CD4+ but not CD8+ cells) and an increase in myeloid cells (macrophages
343 and dendritic cells). We excluded the role of the lymphocytic compartment in the observed
344 phenotype as GSKi pre-treated cancer cells maintained their growth defect in genetically-
345 immunodeficient mice lacking mature lymphocytes (Rag1-/-).
346 Although TAMs did not present distinct expression of canonical pro- or anti- tumour markers
347 between tumours from control and pGSKi cancer cells, RNAseq analysis showed broad
348 changes in their transcriptome. In particular, TAMs from tumours generated by GSKi pre-
349 treated cancer cells suggested an anti-tumour function with a significant increase in Interferon
350 γ (INFγ) signallling. Indeed, TAM infiltrating pGSKi tumours showed clear increase in nuclear
351 pSTAT1, the effector transcription factor downstream of INFγ . We could confirm that this anti-
352 tumorigenic function of TAM was responsible for inhibiting cancer growth in *ex-vivo* and *in vivo*
353 experiments. Interestingly, in *ex-vivo* co-culture, the TAM anti-tumour function was only
354 detected in presence of freshly isolated stromal cells, but this did not depend on their origin,
355 could either be from pGSKi or control tumours. This suggests that fibroblasts might enhance
356 TAM toxicity by providing adhesion for macrophages and increase their proximity to cancer
357 cells and also suggests that macrophage polarization acquired intra-tumorally is a stable
358 phenotype independent from external factors.
359 Finally, when testing the functional role of macrophages on tumour growth *in vivo* we
360 confirmed their anti-tumour function. By using Clodronate, a type of bisphosphonate which
361 once encapsulated into liposomes is up taken by macrophages and mediates their depletion

362 (23), we could clearly see the opposing effects in control or pGSKi tumours in either inhibiting
363 or promoting growth respectively.
364 Thus far, it has been shown how CAFs can contribute to assembling an immunosuppressive
365 TME accordingly to their type of activation (9). We could detect an alteration in pathways
366 responsible with immunomodulation in the TME mesenchymal compartment. We found
367 macrophages infiltrating pGSKi tumours to display increased INFγ-STAT1activation and
368 reduced NFkB signalling. This was shown by the increase in nuclear staining for the
369 INFγ effector pSTAT1 and reduced staining for p65. INFγ signalling is typical of anti-tumour
370 functions in the immune-microenvironment (24), therefore a switch in signalling activation
371 could control macrophage behaviour.
372 Overall, our data shows that cancer cells assemble very specific tumour microenvironments
373 very early in tumour development. The present study reveals a key role of an atypical TME as
374 dominant in inhibiting tumour growth due to the lack of crucial pro-tumoral signals leading to
375 the onset of anti-tumour TAMs (Figure 7). The different TME contains fibroblasts and
376 macrophages with Low Activation of clusters of genes, LA-TME signatures, which allows
377 identification of human breast cancers with better prognosis.
378 Remarkably, the TAMs found in tumours from GSKi pre-treated cells, despite displaying
379 cancer killing activity, do not show canonical M1 markers nor M1 macrophage infiltration was
380 observed in human tumours correlating with the LA-TME signatures. This suggesting that this
381 non-canonical anti-tumour macrophage polarisation might exist in human tumours and
382 contribute to better clinical outcome.
383

384 **Acknowledgments**

385 The graphic representation in the figures were created using BioRender.com.
386 We thank E. Sahai (The Francis Crick Institute) for scientific discussions. We thank Jose L.
387 Orgaz-Bueno, Eva Crosas-Molist, Irene Rodriguez-Hernandez, Stefania di Blasio, Victoria
388 Bridgeman and Emma Nolan for scientific discussions and support during the course of this
389 project. E. Nye from the Experimental Histopathology Unit at the Francis Crick Institute for
390 histological processing and analysis support; J. Bee from the Biological Resources Unit at the
391 Francis Crick Institute for technical support with mice and mouse tissues; R. Goldstone and
392 A. Edwards from the Advanced Sequencing Facility at the Francis Crick Institute for technical
393 support; the Flow Cytometry Unit at the Francis Crick Institute.
394 This work was supported by the Francis Crick Institute, which receives its core funding from
395 Cancer Research UK (FC001112), the UK Medical Research Council (FC001112), and the
396 Wellcome Trust (FC001112) and the European Research Council grant (ERC CoG-H2020-

725492). VSM lab was supported by Cancer Research UK (CRUK) C33043/A24478 and Barts Charity.

Author contributions

A.P.R. designed and performed most of the experiments, analysed and interpreted the data and contributed to the manuscript preparation. O.M. performed tumour staining and quantification analysis of in vivo macrophages, performed secretome data analysis and critically review the manuscript. L.O. assisted with some of the experimental design and critically review the manuscript. P.C. performed bioinformatics analysis. I.M. and V.S.M. designed and supervised the study, interpreted the data and wrote the manuscript.

409 **Figures and Legends**

410 **Figure 1**

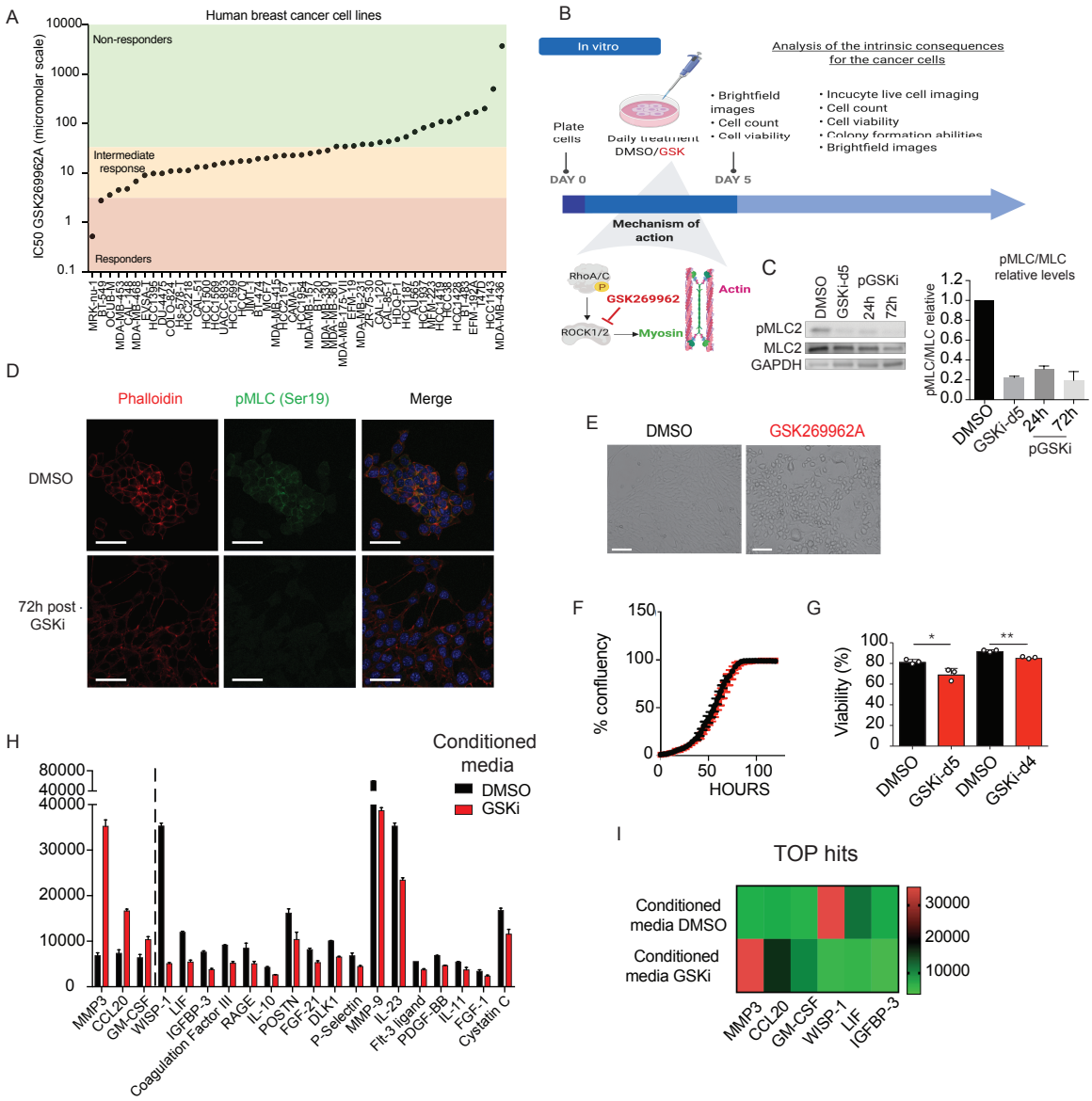

411

412 **Figure 1**

413 **A.** Distribution of GSKi response across human breast cancer cell lines. IC50 of GSK269962A
414 inhibitor across 48 human breast cancer cell lines. Compounds are ranked in descending
415 order of response and divided into responders (IC50<5µM, red), intermediate response (IC50
416 5-50µM, orange) and non-responders (IC50 >50µM, green). **B.** Schematic of the experimental
417 setup for the characterisation of the intrinsic effects of GSK269962A on cancer cells. Cancer
418 cells were plated and treated daily with vehicle (DMSO) or 5 µM of GSK269962A GSK1/2
419 inhibitor (GSK1) for five days. **C.** Western blot analysis of Phospho-MLC (pMLC) after 5 days
420 of GSKi treatment (5 Days), 24h or 72h post-treatment. (Left panel) Quantifications of relative
421 pMLC2 levels in 4T1 cells as a fold change versus the control from two independent

experiments (right panel) **D.** Immunofluorescence images of pre-treated 4T1 cells 72 hours after treatment was removed. Cytoskeleton was stained using phalloidin (red), contractility using pMLC (green) and nucleai using DAPI (blue). (Scale bar 50μm). **E.** Representative brightfield images of 4T1 cells following a 5-day treatment with GSK269962A inhibitor. (Scale bar 100μm). **F.** Growth curve of cells pre-treated with DMSO (black) or GSK269962A inhibitor (red). Cell confluency was monitored every 3 hours for <120 hours using Incucyte. **G.** Percentage of cell viability quantified after 5 days of treatment and at day 4 post-treatment: DMSO (black) or GSK269962 (red) for 5 days. Error bars represent the SEM from three independent experiments. Statistic, Student's t-test (*$p < 0.05$, ** $p < 0.01$). **H.** Quantification of differentially secreted factors in the conditioned media using Protein Array () of pre-treated 4T1 cells, 48 hours after treatment. Error bars represent SEM from two technical replicates. **I.** Heatmap of the top 3 upregulated (red) and downregulated (green) factors in GSK269962A-conditioned media.

436 **Figure 2**

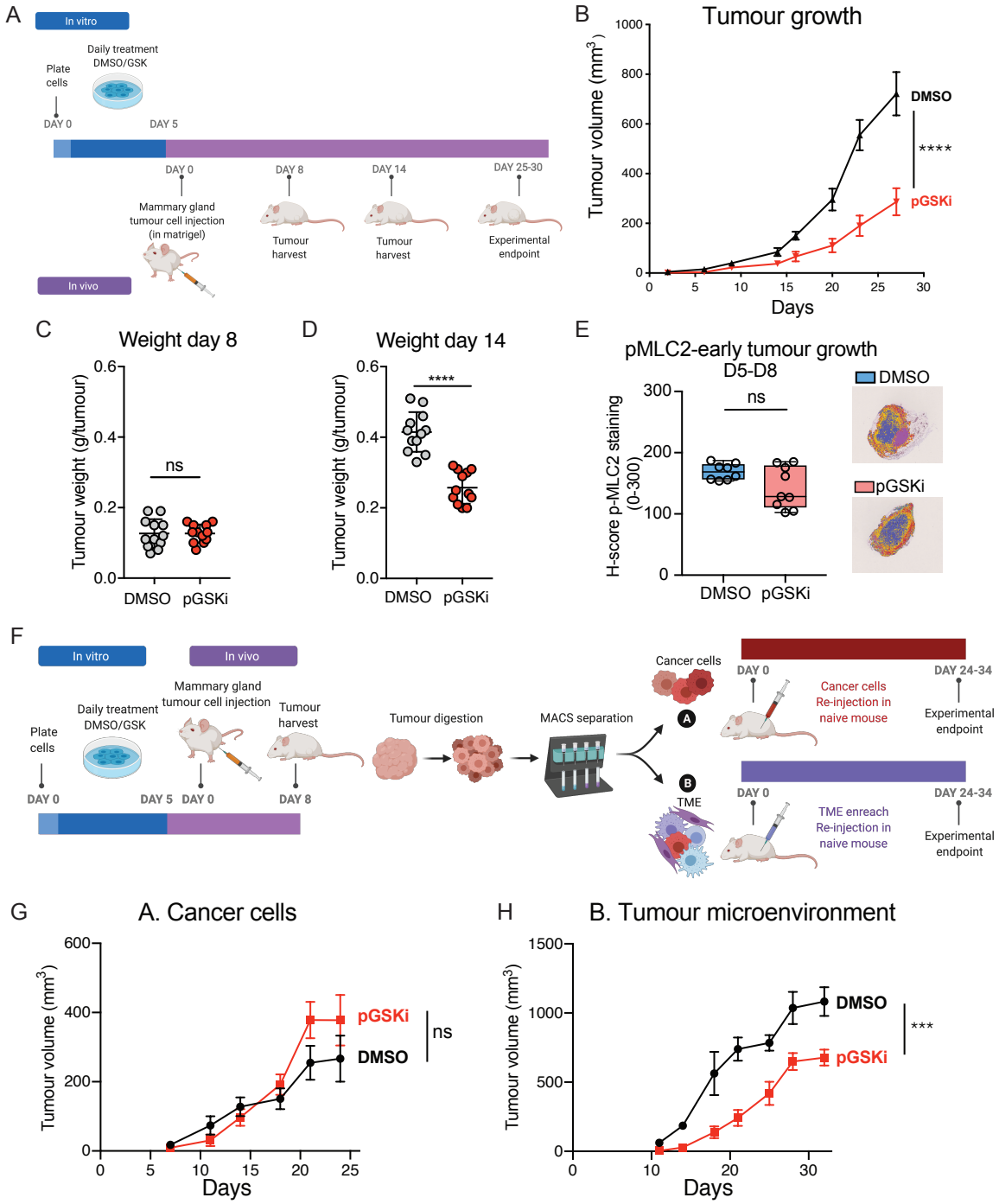

437

438 **Figure 2**

439 **A.** Schematic of the experimental setup. **B.** Mean tumour volume over time of tumours
440 generated by 4T1 cells pre-treated with DMSO (black) or GSK269962A (red) in the fat pad of
441 Balb/cAnN mice. Error bars represent SEM from four independent experiments (total of n=20
442 tumours). Statistic two-way ANOVA with Sidak's multiple comparisons test **C-D.** Histogram of
443 tumour weight at day 8 (n=28) (C) and day 14 (n=12) (D). Statistic: Student's t-test between
444 DMSO and GSK269962A groups. Statistically significant (ns: not significant, **** $p < 0.0001$

445 **E.** (Left) H-score of p-MLC2 staining in 4T1 tumour-derived cells pre-treated with DMSO (blue)
446 or GSK269962A (red) from days 5 and 8 (Right) Representative QuPath color-maps of pMLC2
447 staining in both conditions. **F.** Schematic of the experimental setup. Day 8 tumours were
448 separated by magnetic cell sorting into (A) cancer cells (hCD2+) and (B) tumour
449 microenvironment (TME, hCD2-). Each of the components, was separately injected into new
450 naïve Balb/cAnN mice. **G.** Mean tumour volume of (A) 4T1 cells isolated from day 8 DMSO
451 (black) or GSK269962A (red) tumours. Error bars represent SEM from two independent
452 experiments (n=9 total number of tumours). **H.** Mean tumour volume of (B) TME cells isolated
453 from day 8 DMSO (black) or GSK269962A (red) tumours. Error bars represent SEM from two
454 independent experiments (n=7 total number of tumours). Data were analysed using two-way
455 ANOVA. (ns: not significant, *** $p < 0.001$).
456

Figure 3

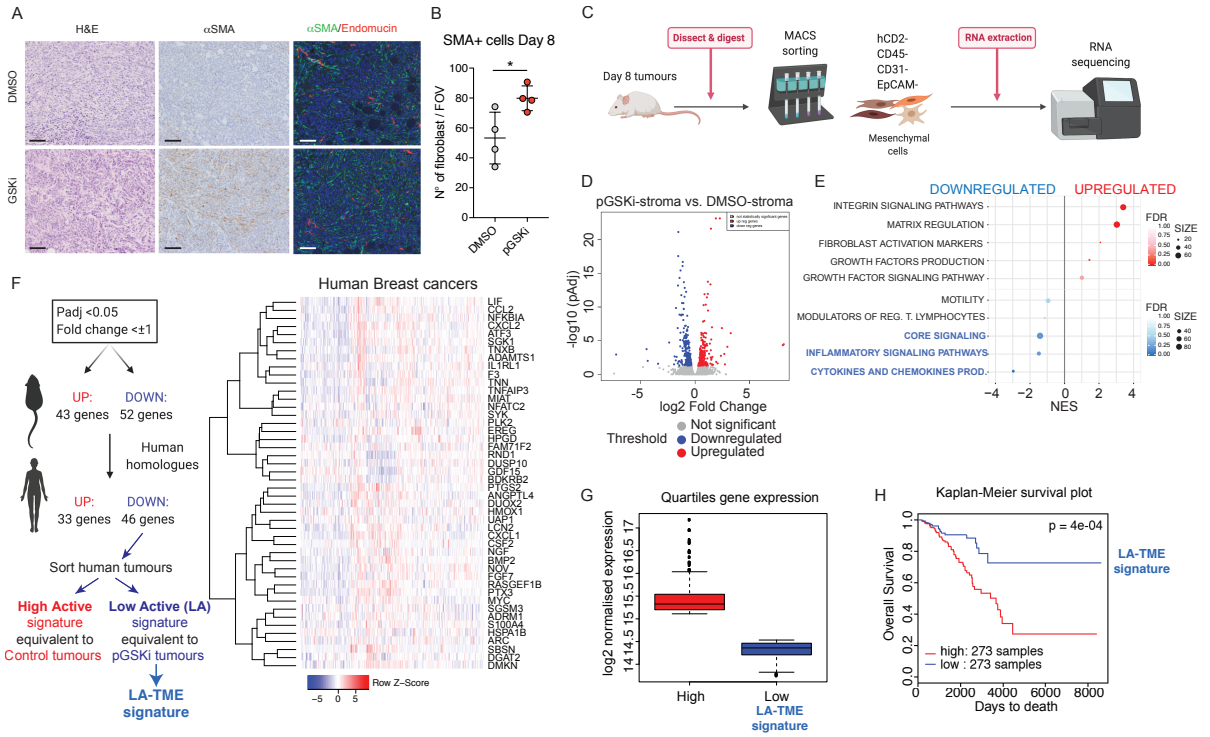

Figure 3

A. Representative IHC images of orthotopic syngeneic tumours 8 days post-transplantation from 4T1 pre-treated with DMSO or GSKi. Hematoxilin/Eosin (left), αSMA antibody DAB-staining (middle) and fluorescence double staining of αSMA (green), Endomucin (red) and DAPI (blue) to stain the nuclei (right) (Scale bar 100μm). **B.** Quantification of αSMA+Endomucin- cells in DMSO or GSKi pre-treated tumours 8 days post-transplantation. Error bars represent the SEM from 4 tumours with 6 fields of view (FOV)/tumour. Data were analysed using a student's t-test (*$p < 0.05$). **C.** Experimental design for tumour associated mesenchymal cell isolation. **D.** Volcano plot comparing the gene expression profile of stromal cells derived from GSKi vs. DMSO pre-treated tumours. Statistical significance (-log10 adjusted pvalue) against foldchange (log2) of fibroblasts derived from GSKi vs. DMSO pre-treated tumours. Significantly upregulated genes are shown in red and downregulated genes are shown in blue. **E.** Gene signatures in CAF-specific molecular mechanisms were selected and ranked (upregulated in red; downregulated in blue). Gene-expression differences are displayed as a normalised enrichment score (NES), and false discovery rate (FDR) is used to determine the significance of each pathway. The size of the circle represents the number of genes within each signature that are differentially expressed in GSKi vs. DMSO-CAFs. **F.** (Left panel) Schematic representation of how the Cancer Low Contractility (CLC) - TME signature was generated stemming from genes downregulated in tumour initiated by cancel cells with reduced contractility (GSKi). Padjusted value (Padj) and log2 fold change (fold change) were

479 used as cut-offs for gene selection. (Right panel) Heatmap of the 46 genes that constitute the
480 CLC-TME signature and their expression across 1092 breast cancer tumours from the TCGA
481 cohort. **G.** Log2 expression of the CLC-TME signature divided patients into high (red,
482 equivalent to signature in mouse control tumours) and low (blue, equivalent to signature in
483 mouse GSKi tumours) quartiles. Box-an-whisker plots showing median centre line, 25% and
484 75% box limits and rang of expression. **H.** Kaplan-Meier curve represents the overall survival
485 of 546 breast cancer patients from the TCGA cohort subdivided into high (red) and low (blue)
486 expression of the GSKi-CAF "down signature". Data were analysed using a Wald test and
487 statistically significant changes between the two groups are indicated (* $p < 0.05$) (hazard ratio
488 is 1.96 and confidence intervals are 1.1 – 3.93).
489

490 **Figure 4**

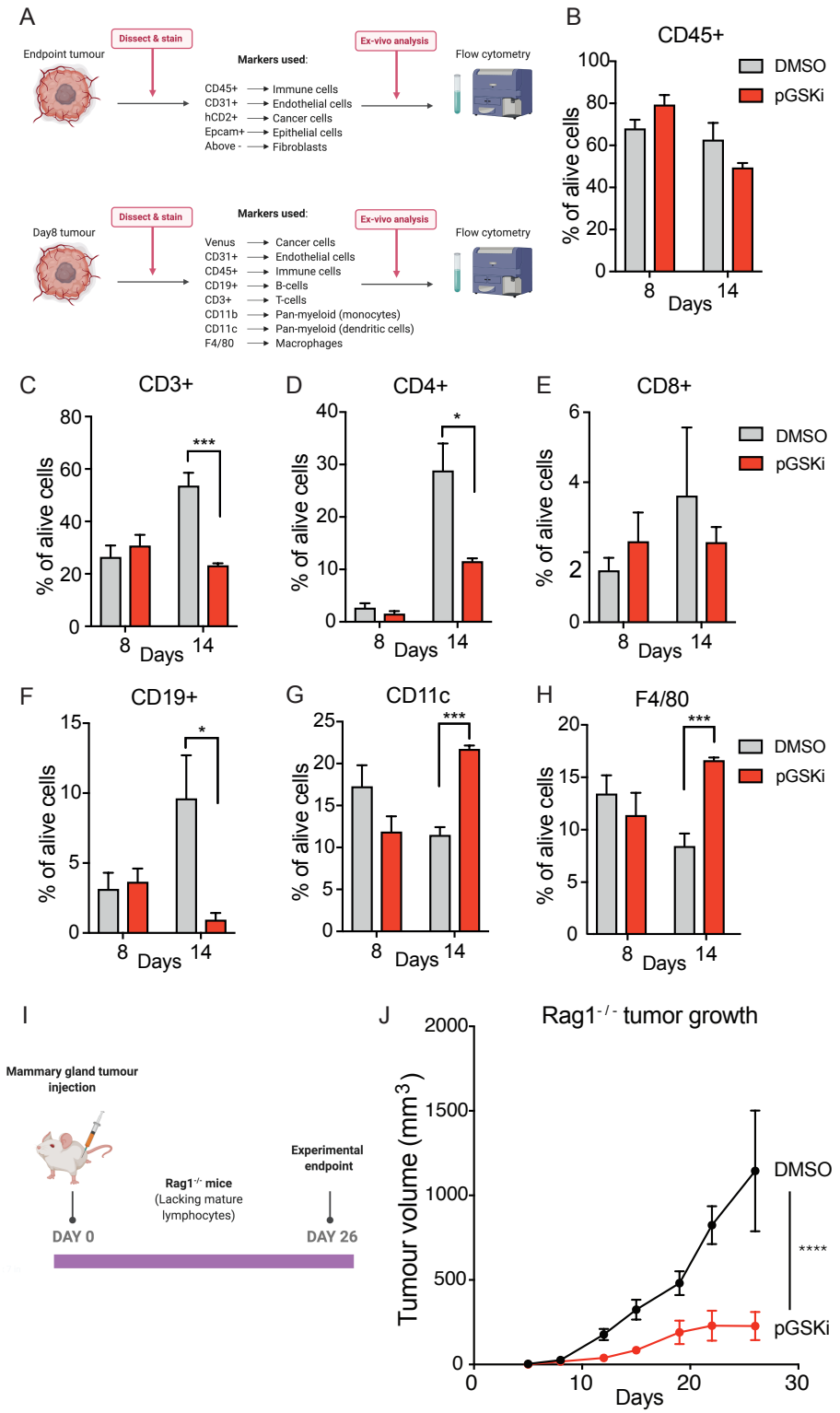

491

492 **Figure 4**

493 **A.** Experimental design and antibodies used for detecting immune cells populations within the
494 TME. **B-H.** Flow cytometric quantification of TME cell frequencies out of the total alive cells
495 lungs in mice harbouring DMSO (grey) or GSK269962A (GSKi) (red) pre-treated tumours at

496 the indicated times post-injection. (B) total CD45+ immune cells (C) CD45+CD3+ T-cells; (D)
497 CD45+CD4+ T-cells; (E) CD45+CD8+ T-cells; (F) CD45+CD19+ B-cells; (G) CD45+CD11c+
498 dendritic cells; (H) CD11b+F4/80+ macrophages. Error bars represent the SEM from two
499 independent experiments (Total n=12 in each group). Data were analysed using a t-test
500 between DMSO and GSKi groups at each time points. (* $p < 0.05$, *** $p < 0.001$). **I.** Diagram
501 of the experimental design. **J.** Mean tumour volume of 4T1 cells grown over 26 days. Tumours
502 were pre-treated in vitro with DMSO (black) or GSKi (red). Error bars represent the SEM from
503 two independent experiments (total of n=12 (DMSO) and n=10 (GSKi)). Data were analysed
504 using a two-way ANOVA (**** $p < 0.0001$).
505

506 **Figure 5**

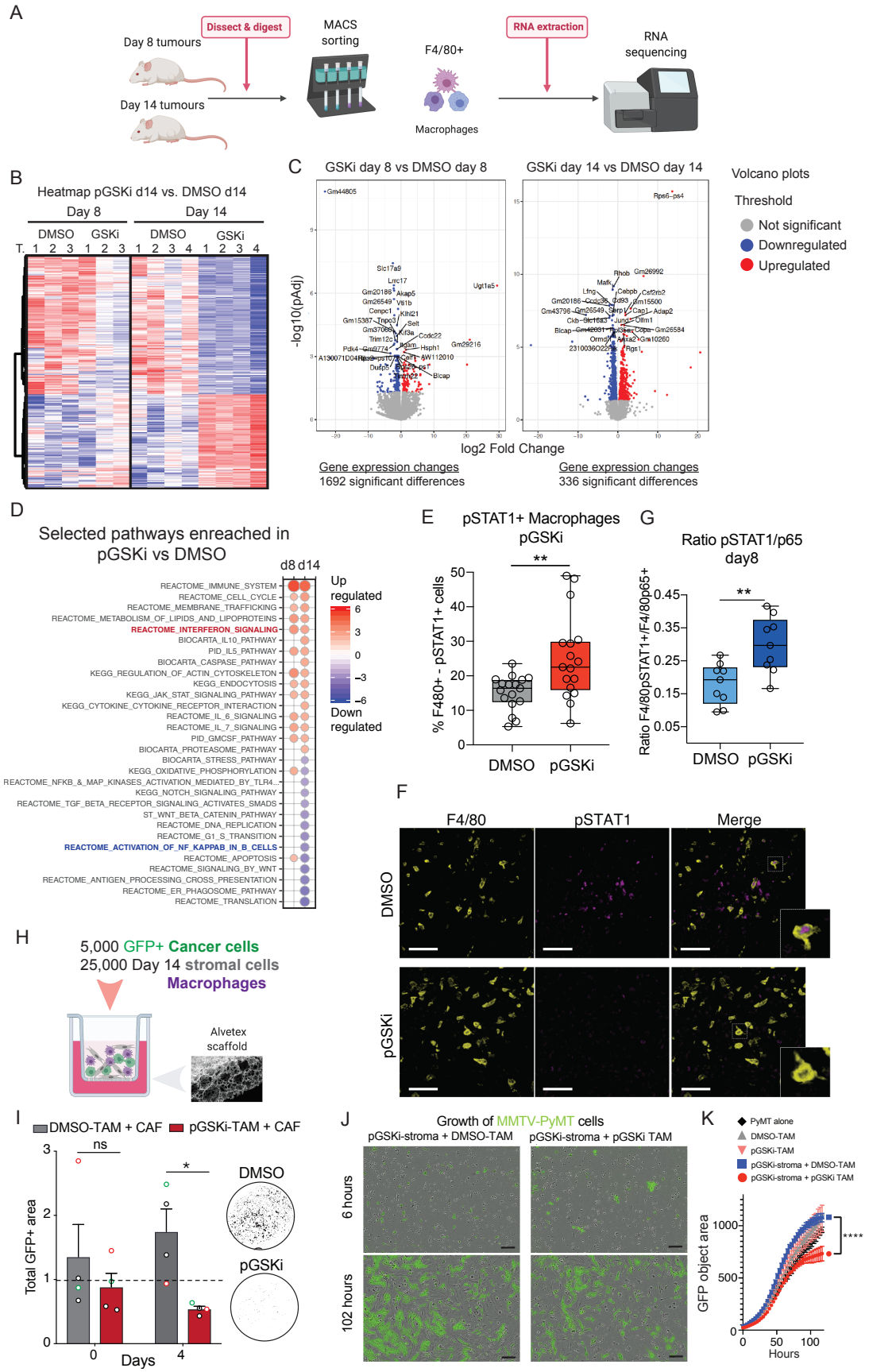

507

508 **Figure 5**

509 **A.** Schematic representation of the experimental design and sample collection. **B.** Heatmap
510 comparing the gene expression profile of macrophages derived from GSKi vs. DMSO pre-
511 treated tumours 8 and 14 days post-transplantation. **C.** Volcano plots of statistical significance
512 (-log10 adjusted pvalue) against foldchange (log2) of macrophages derived from GSKi vs.
513 DMSO day 8 pre-treated tumours (Left) or day 14 pre-treated tumours (Right). Significantly
514 upregulated genes are shown in red and downregulated genes are shown in blue. **D.** Summary
515 of selected pathways enriched in GSKi vs. DMSO. Upregulated or downregulated pathways
516 at the indicated time point are indicated in in red and blue respectively.

517 **E.** Percentage of pSTAT1 positive macrophages derived from DMSO (grey) or GSKi (red)
518 pretreated tumours from day 14. **F.** Representative staining of F4/80 (yellow) and pSTAT1
519 (Magenta) of DMSO or GSKi pre-treated tumours section (Scale bar 50μm). **G**. Ration
520 between p65 and pSTAT1 staining in macrophages in tumour pre-treated with DMSO (gray)
521 or GSKi (red) from day 8. **H.** Experimental design of the co-culture. **I.** Quantification of primary
522 MMTV-PyMT-GFP+ cell growth by measuring the total GFP+ area over the course of 4 days.
523 Cells were grown with DMSO-Macrophages and CAFs (grey) or GSKi-macrophages and
524 CAFs (red) from 14-days tumours and normalised to the growth of MMTV-PyMT cells alone
525 (dash line). Representative fluorescence pictures are shown. Error bars represent the SEM
526 from three independent experiments shown with black, green or red data points. Biological
527 replicates within each experiment are indicated in the graph. Data were analysed using a
528 Student's t-test (* $p < 0.05$). **J.** Representative brightfield images of MMTV-PyMT-GFP+ cells
529 (green) in co-culture with GSKi-CAFs and either DMSO (left) or GSKi (right) macrophages.
530 Timepoints are indicated. Scale bar, 30 μm. **K.** Quantification of MMTV-PyMT-GFP+ cell area
531 when cells were grown alone (black), with macrophages from DMSO (grey) or GSKi (coral)
532 pre-treated tumours or with CAFs from GSKi pre-treated tumours and macrophages extracted
533 from either DMSO (blue) or GSKi (red) pre-treated tumours. Statistic two-way ANOVA (blue
534 vs red) (**** $p < 0.0001$).

535

536 **Figure 6**

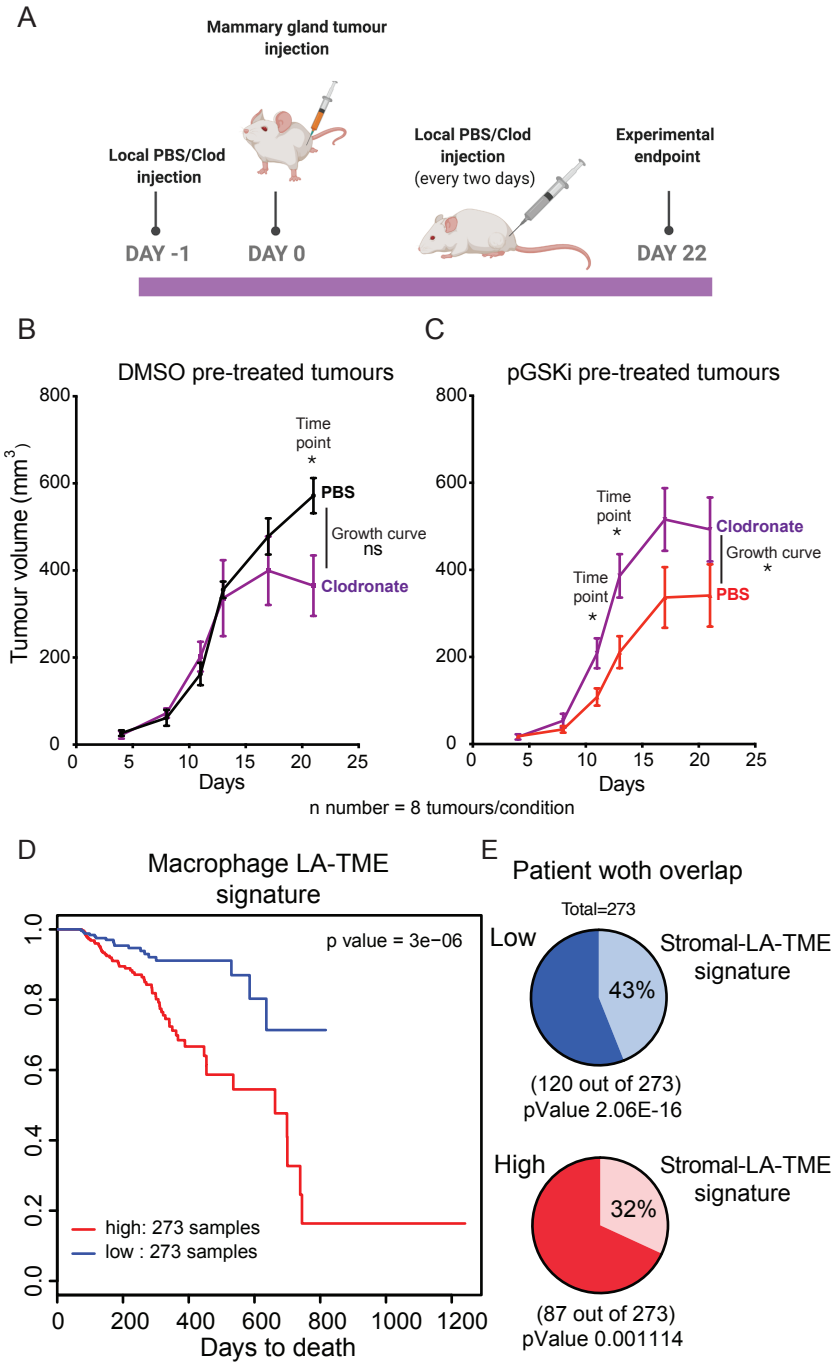

537

538 **Figure 6**

539 **A.** Experimental design. **B-C.** Mean volume of 4T1 tumours over 22 days. 4T1 tumour cells
540 were pre-treated in vitro with DMSO (B) or GSK inhibitor (C), and tumours were treated with
541 either PBS liposomes (black and red lines) or clodronate liposomes (purple lines). Error bars
542 represent the SEM (n=8 tumours per condition). Data were analysed using a two-way ANOVA
543 comparing the curves (at the end of the curves) (ns: not significant, * $p < 0.05$) and t-tests at
544 individual timepoints when significant difference were present (indicated above each time

545 point) (* $p < 0.05$). **D.** Kaplan-Meier curve represents the overall survival of 546 breast cancer
546 patients from the TCGA cohort subdivided into high (red) and low (blue) expression of the
547 macrophage signature. Data were analysed using a Wald test and statistically significant
548 changes between the two groups are indicated (* $p < 0.05$) (hazard ratio is 1.96 and confidence
549 intervals are 1.1 – 3.93). **E.** Pie charts represent the overlap between patients with both
550 alternative macrophage and alternative stromal signatures from GSKi pre-ptreated tumours.
551

552 **Figure 7**

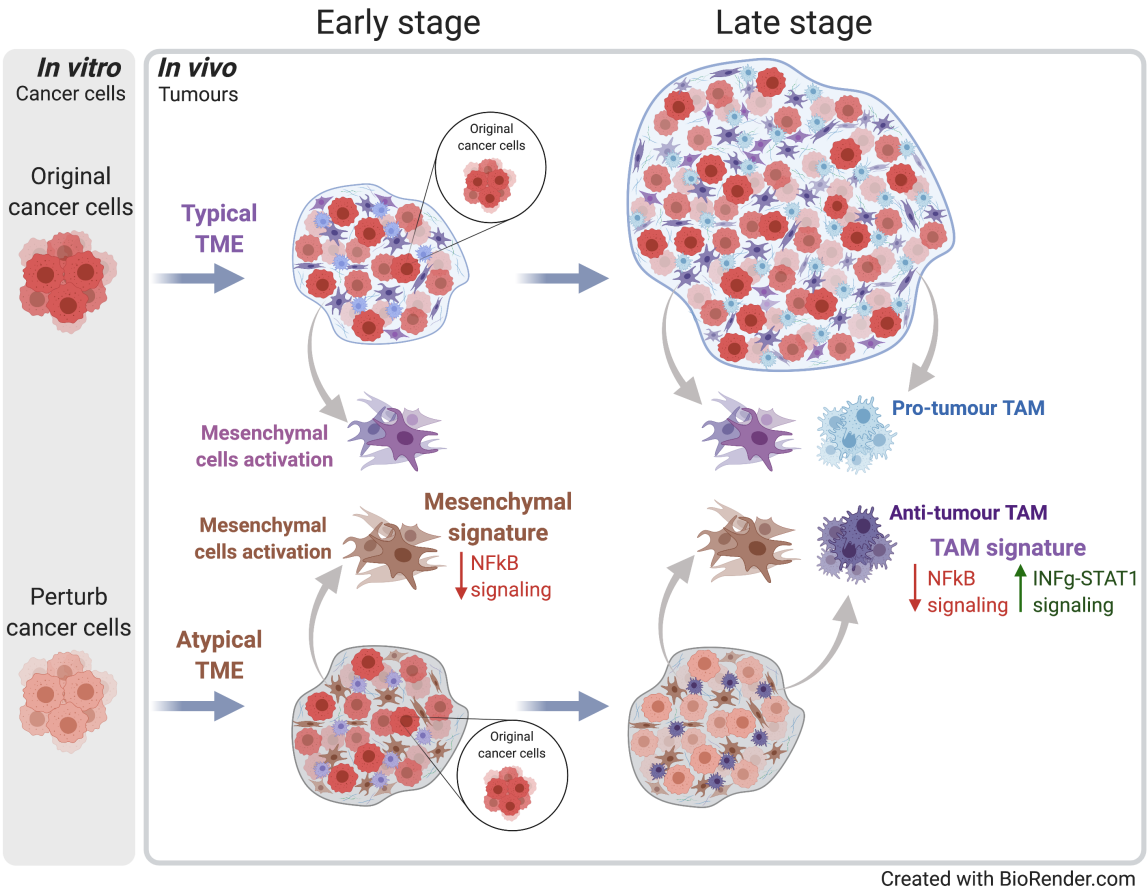

553

554 **Figure 7**

555 Graphic summary: breast cancer cells with initial reduced GSK-Myosin II activity generated
556 an alternative early TME characterized by alternative Carcinoma Activated Fibroblasts (CAFs)
557 displaying a Cancer Low Contractility (CLC)-CAF-signature. The CLC-CAF-signature show
558 overall reduced pro-inflammatory activity including down-regulation of NFκB signalling. The
559 alternative TMA fails to sustain pro-tumourigenic signalling typical of Tumour Associated
560 Macrophages (TAM), which consequently display a CLC-TAM-signature with reduced pro-
561 tumoural NFκB signalling and anti-tumour Interferon Gamma (INFγ), STAT1^{high} activity. These
562 macrophages -lacking canonical M1 markers- reduced long-term tumour growth.

563

564

Supplementary Figures and Legends

Supplementary Figure 1

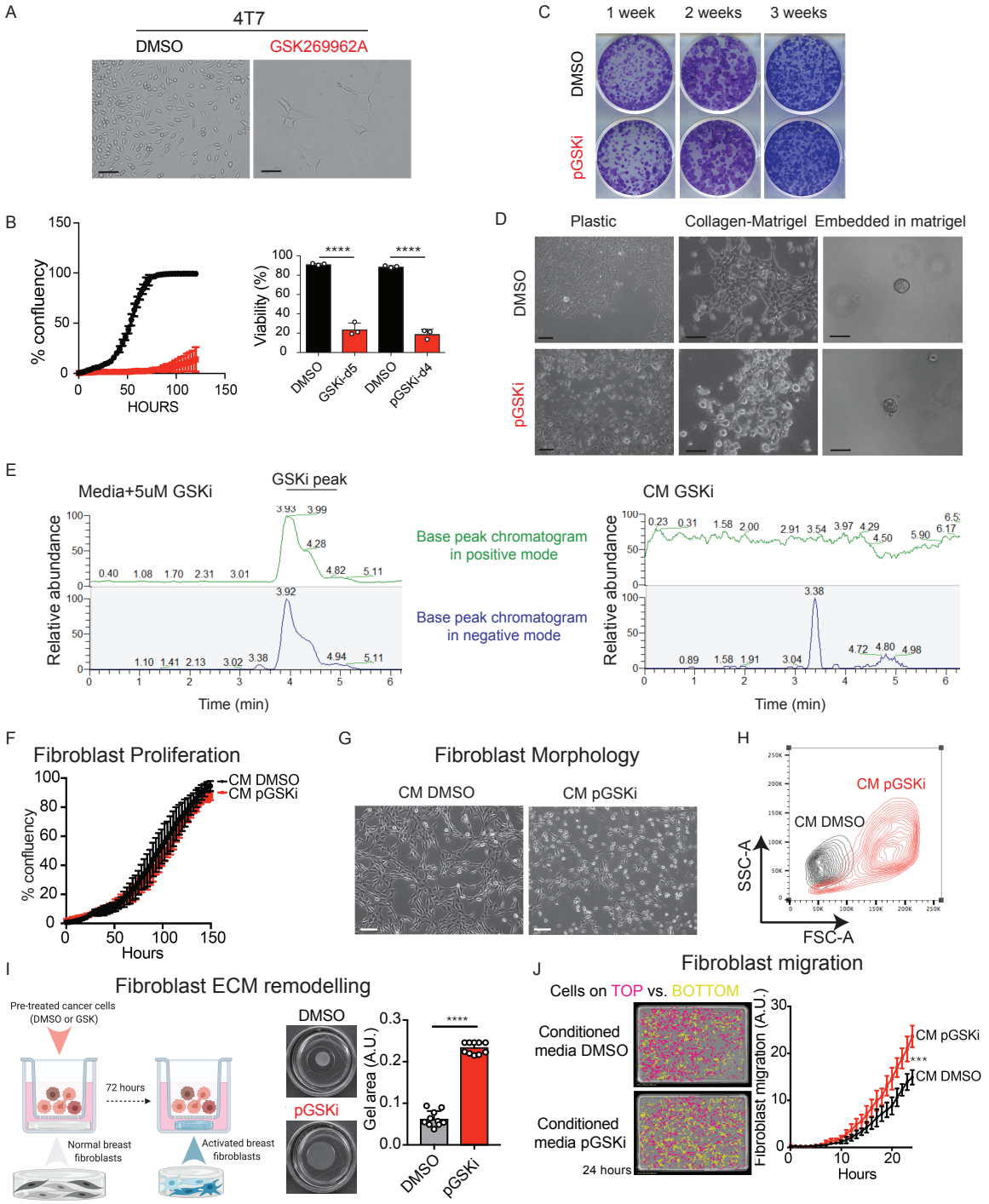

Supplementary Figure 1

A. Representative brightfield images of 4T07 cells following a 5-day treatment with GSKi. **B.** (Left) Growth curve of cells pre-treated with DMSO (black) or GSKi (red). Cell confluency was monitored every 3 hours for <120 hours using Incucyte. (Reft) Percentage of cell viability quantified at 5 days after treatment and at day 4 post-treatment: DMSO (black) or GSKi (red)

573 for 5 days. (Scale bar 100μm). (B-D) Error bars represent the SEM from three independent
574 experiments (dots). Student's t-test analysis between DMSO and GSKi groups (**** $p <$
575 0.0001). **C.** Representative image of the surviving fraction of 4T1 breast cancer cell lines pre-
576 treated with DMSO (black) or GSKi (red) following weekly re-plating and during three
577 consecutive weeks. **D.** Representative bright-field images of pre-treated 4T1 cells with DMSO
578 (upper panels) or GSKi (lower panels) plated on plastic (Left), on a CollagenI-matrigel matrix
579 (Middle) or embedded in matrigel (Right). (Scale bars 50μm). **E.** Liquid chromatography-mass
580 spectrometry chromatograms on positive mode (green) or negative mode (blue) on media
581 containing 5uM of GSKi as positive control (Left) and the 4T1-GSKi pre-treated conditioned-
582 media (Right). The detection limit of 0.01nM was experimentally determined by diluting the
583 positive control. **F.** Growth curve of mNBFs incubated with DMSO (black) or GSKi (red)
584 conditioned media. Cell confluency was monitored every 3 hours for <150 hours using
585 Incucyte. Data were analysed using two-way ANOVA test (ns: not significant). **G.**
586 Representative brightfield images of (mNBF) cell morphology following a 2-day incubation with
587 conditioned media (CM) from DMSO or GSKi pre-treated 4T1 cells. (Scale bar 100μm). **H.**
588 Flow cytometric analysis of the size of mNBFs from (B) based on forward/side scatter. **I.** (Left)
589 Schematic representation of the set-up for fibroblast contraction assays, (middle)
590 representative pictures and (right) quantification of fibroblast contraction assays with DMSO
591 (black) or GSKi (red) pre-treated 4T1 cells. Error bars represent the SEM from three
592 independent experiments and technical repeats (Total n=10 per condition). Student's t-test
593 analysis (**** $p< 0.0001$). **J.** (Left) Representative example and (right) quantification of a
594 murine normal fibroblast mNBF chemotaxis migration assay towards DMSO (black) or GSKi
595 conditioned media from 4T1 pre-treated cells. Fibroblast migration data was acquired every
596 hour for 24 hours using Incucyte and the values are given in arbitrary units (A.U.). Data were
597 analysed using two-way ANOVA test (*** $p < 0.001$).
598
599

600 **Supplementary Figure 2**

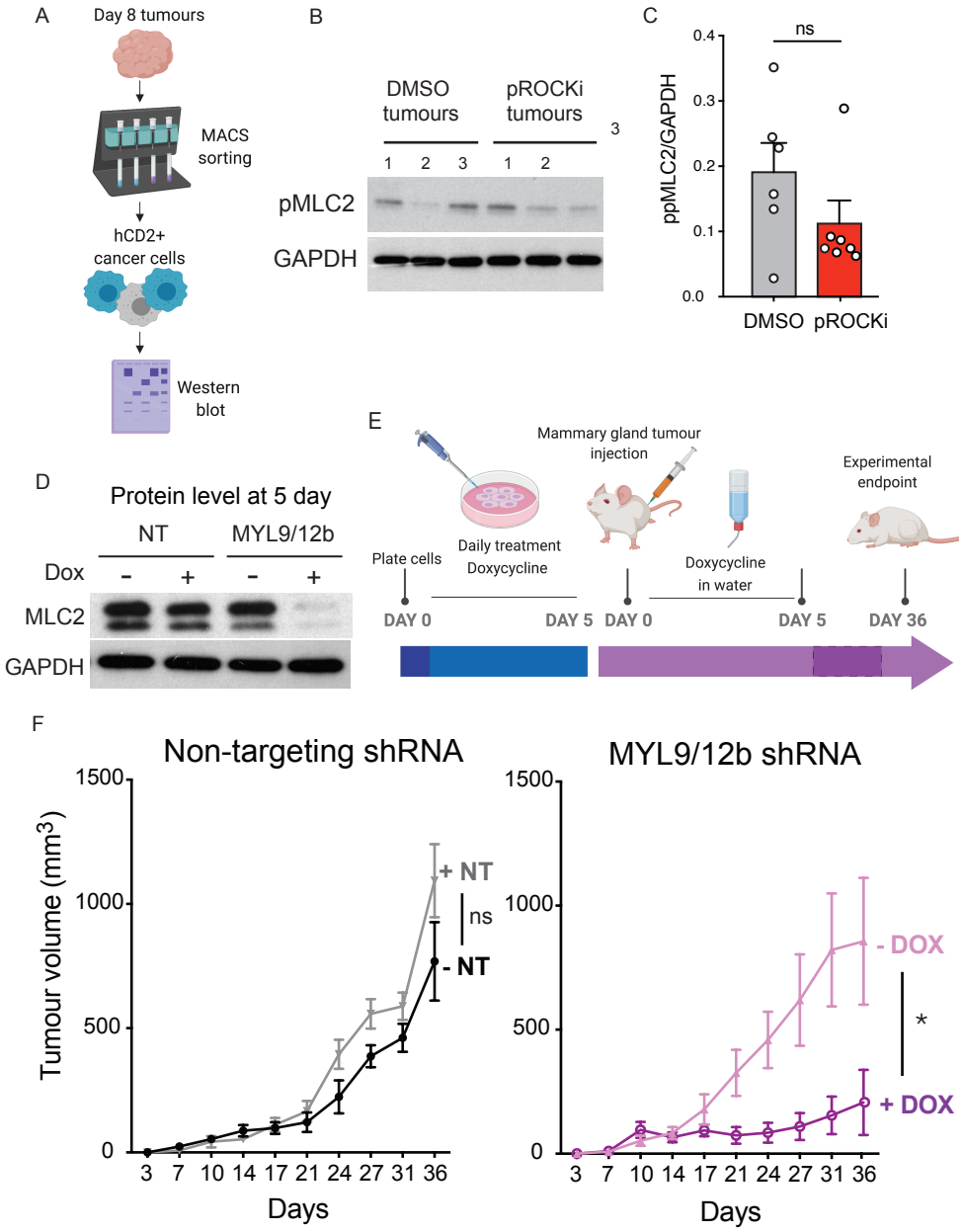

601

602 **Supplementary Figure 2**

603 **A.** Schematic of sample collection workflow where hCD2+ cancer cells were isolated from
604 tumours before performing a western blot. **B.** Representative western blot of pMLC2 and
605 GAPDH as loading control in 4T1 pre-treated cells isolated from day 8 tumours. **C.**
606 Quantification of relative ppMLC2 levels in 4T1 tumour-derived cells pre-treated with DMSO
607 (black) or GSKi (red). Error bars represent the SEM from two independent experiments (total
608 n=6-7 tumours). Student's t-test analysis (ns=non-significant). **D-E.** Western blot analysis of
609 MLC2 after 5 days of DOX treatment *in vitro*. (D). Schematic of the experimental setup:
610 Doxycyline was administered to the cells *in vitro* and *in vivo* during the first five days post-

transplantation into the fat pad of Balb/cAnN mice (E). **F.** Mean tumour volume of 4T1 cells transduced with a hairpin inducible vector for Non-targeting (black/grey) or MYL9/12b-targeting shRNA (purple, pink). Error bars represent SEM from two independent experiments (n=8 total number of tumours). Data were analysed using two-way ANOVA with Sidak's multiple comparisons test. (ns: not significant, * $p < 0.05$). **I.** Error bars represent the SEM from three independent experiments (total n=17 tumours/condition). Student's t-test analysis (**** $p < 0.0001$).

Supplementary Figure 3

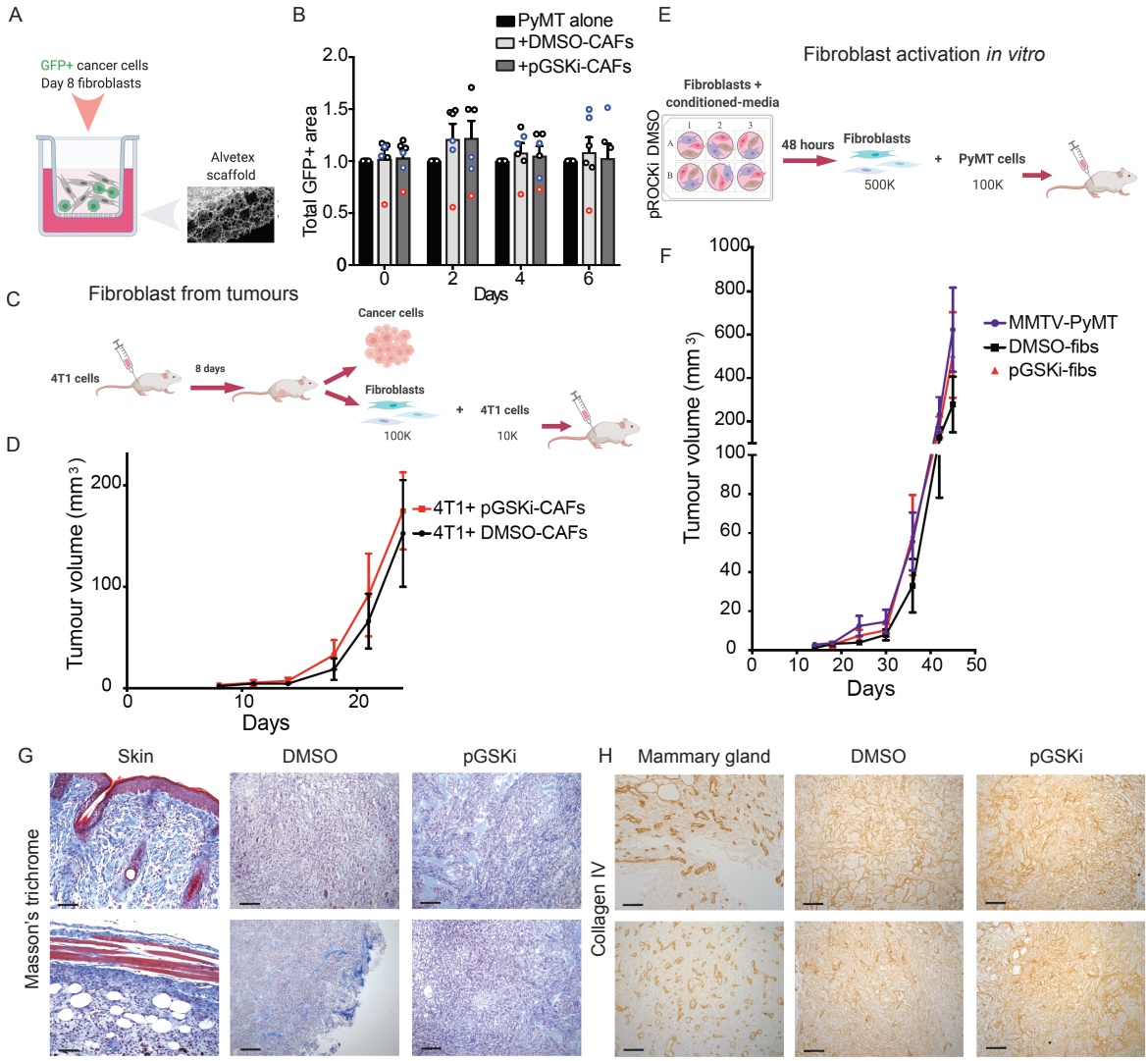

Supplementary Figure 3

A. Experimental design of co-culture on Alvetex scaffolds. **B.** Quantification of MMTV-PyMT-GFP+ cell growth using the total GFP+ area as a readout. Cells were grown alone (black), with DMSO-CAFs (light grey) or GSKi-CAFs (dark grey). Error bars represent the SEM from three independent experiments shown data points. Biological replicates within each experiment are indicated with black, blue or red in the graph. Student's t-test analysis (ns=non-significant). **C-D.** Diagrams of the experimental design indicating the tumour origin of the CAFs before co-injection with cancer cells (C). Mean tumour volume of 4T1 cells co-injected with DMSO-CAFs (black) or GSKi-CAFs (red) and grown over 24 days (D). Error bars represent the SEM (n=6), Data were analysed using two-way ANOVA (ns=non-significant). **E-F.** Experimental design to generate activated fibroblasts in vitro before co-injection with cancer cells (E). Mean tumour volume of MMTV-PyMT cells alone (purple) or co-injected with DMSO-fibroblasts (black) or GSKi-fibroblasts (red) and grown over 45 days (F). Error bars represent

634 the SEM (n=6). Data were analysed using two-way ANOVA (ns=non-significant). **G.**
635 Representative IHC images of 4T1 tumours 8 days post-injection stained with Masson's
636 thricrome staining, marking keratin and muscle fibers (red), collagen (blue), and cell nuclei
637 (dark purple). Skin was used as a staining control. **H.** Representative IHC images of 4T1
638 tumours 8 days post-injection stained collagen IV staining (brown). Normal mammary gland
639 tissue was used as a control.
640

641 **Supplementary Figure 4**

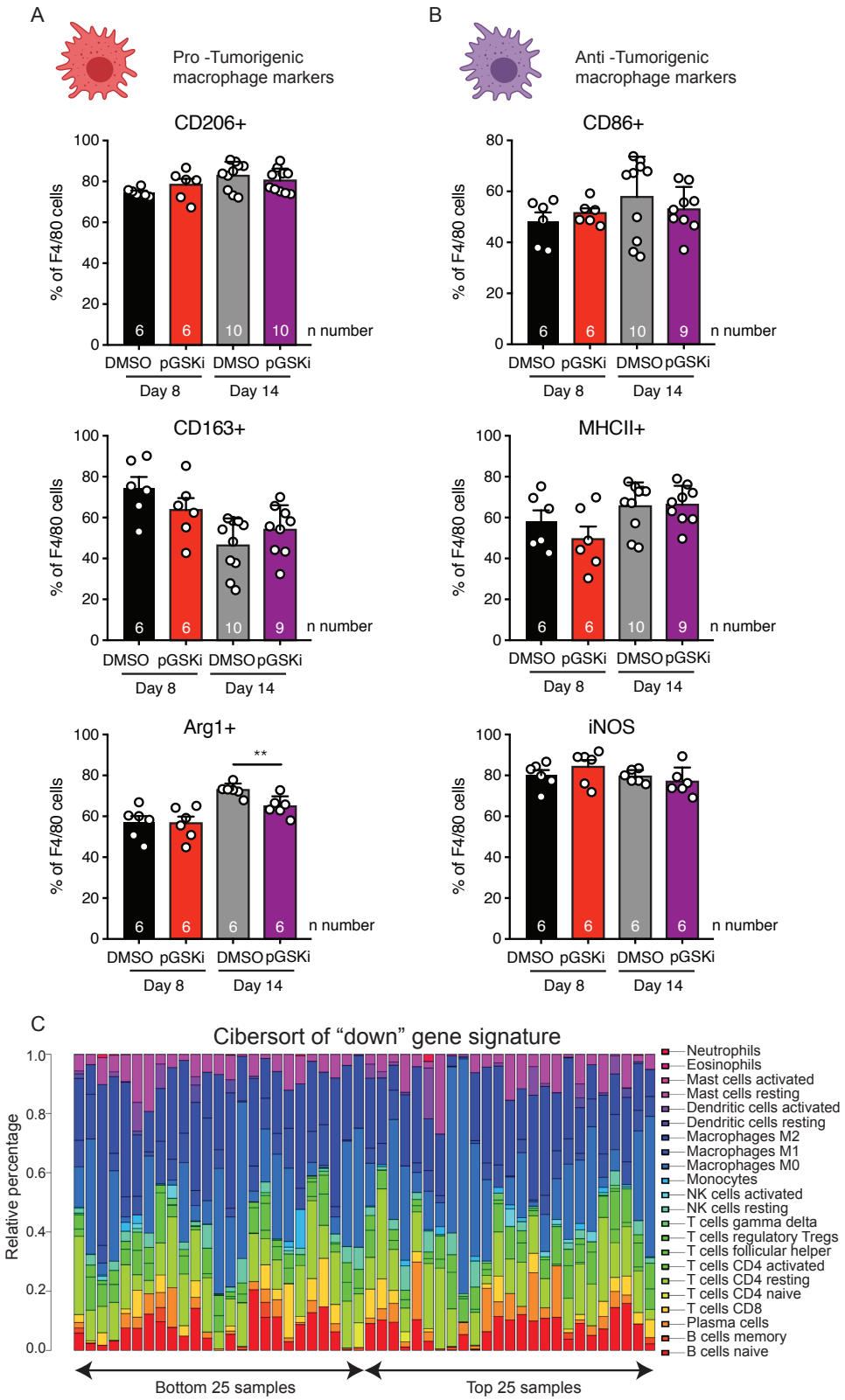

642

643 **Supplementary Figure 4**

644 **A-B.** Flow cytometric quantification of pro-tumorigenic (CD206, CD163 and Arg1) (A) and anti-

645 tumorigenic (CD86, MHCII and iNOS) (B) macrophage polarisation markers 8 and 14 days

post-transplantation. Cells were gated on alive F4/80+ and error bars represent the SEM from two independent experiments (n numbers indicated under each graph). Data were analysed using t-test (** $p < 0.01$). **C.** Cibersort analysis of the relative percentage of immune cell populations in the 25 patients with higher (right – top samples) and lower (left - bottom samples) cumulative gene expression for the down fibroblast signature from Figure 3G. Analysis was performed in the TCGA cohort, and the figure legend (right) indicates the cell populations investigated.

655 **Supplementary Figure 5**

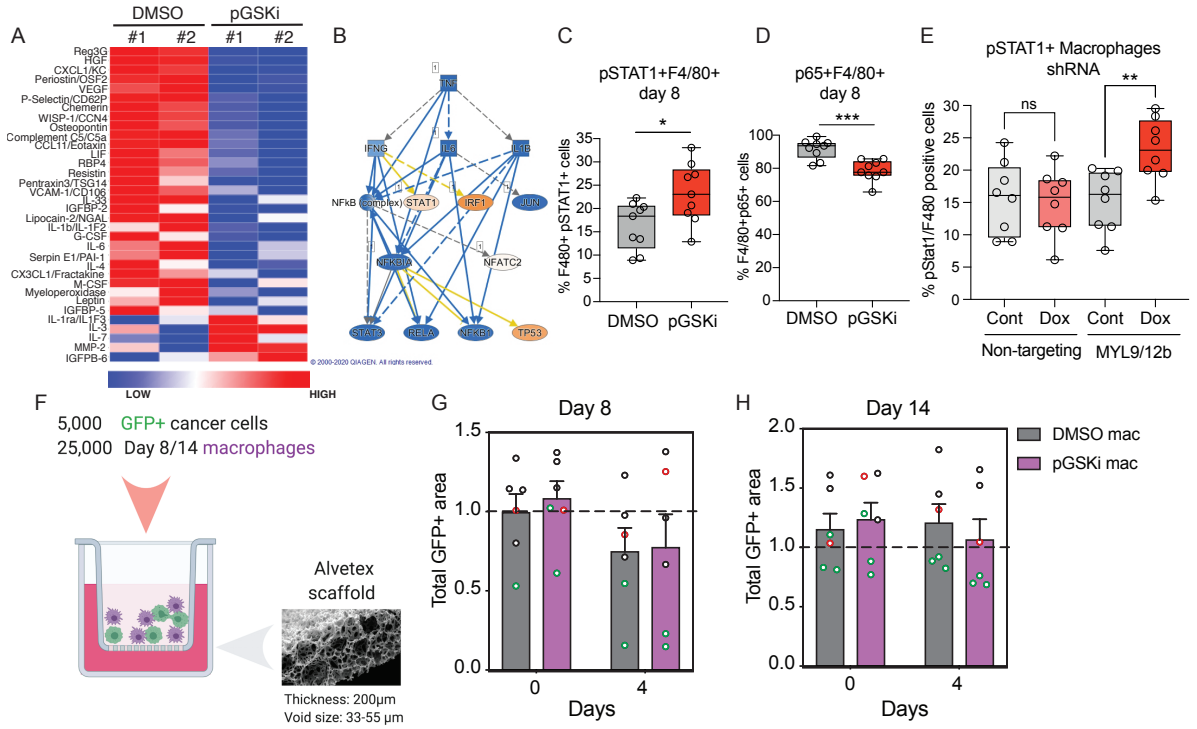

656

657 **Supplementary Figure 5**

658 **A.** Heatmap displaying top differentially secreted factors in the fibroblasts from DMSO and
659 GSKi-pre-treated (GSK) tumours at 14 days using comparative marker selection in
660 GennePattern. **B.** Network analysis enriched in GSKi-pre-treated fibroblasts using Ingenuity
661 pathway analysis (RNA signature from Figure 3D). **C.** Percentage of pSTAT1 positive
662 macrophages derived from DMSO (grey) or GSKi (red) pretreated tumours from day 8. **D.**
663 Percentage of p65 positive macrophages derived from DMSO (grey) or GSKi (red) pretreated
664 tumours from day 8. **E.** Percentage of pSTAT1 positive macrophages derived from control or
665 DOX treated of non-targeting or MYL9/12b-targeting shRNA (Fig. 2F-H). **F.** Experimental
666 design of the co-culture. **G-H.** Quantification of MMTV-PyMT-GFP+ cell growth by measuring
667 the total GFP+ area as a readout over the course of 4 days. Cells were grown with DMSO-
668 Macrophages (grey) or GSKi-macrophages (purple) from day 8 (G) or day 14 (H) tumours and
669 normalised to the growth of MMTV-PyMT cells alone (dash line). Error bars represent the
670 +SEM from three independent experiments. Biological replicates within each experiment are
671 indicated with black, green or red data points in the graph. No statistically significant changes
672 were observed between groups following student's t-test analysis.

673

674

675

Material and Methods

Data Availability

The RNaseq datasets generated during this study are available will be made available at the Gene Expression Omnibus and they can currently be provided to the reviewers upon requests.

Statistical analysis

Unless otherwise stated, statistical analyses were performed using Prism v.7.0c (GraphPad Software). For column bar or scatter dot plots, error bars are the average ± Standard error of the mean (SEM). Boxplots show min to max values or 10-90 percentile. P values were obtained by Student t-tests with paired or unpaired samples when analysing the differences in one variable between two experimental groups. Two-way ANOVA was used where indicated to perform multiple variable analyses or multiple comparisons between experimental groups. Significance was set at $P < 0.05$ and either the actual P value or symbols describing it (*, $p<0.05$; **, $p<0.01$; ***, $p<0.001$; ****, $p< 0.0001$) are displayed in graphs.

Data were pooled from at least two independent experiments and the exceptions are specified in the respective figure legends. n values represent biological replicates, with the exception of the 3D Alvetex scaffold assays, for which both technical and biological replicates are shown.

Bioinformatic analysis

Gene expression data were analysed by the Bioinformatics & Biostatistics facility at the Francis Crick Institute.

Biological replicate libraries were prepared using the polyA KAPA mRNA HyperPrep Kit and sequenced on Illumina HiSeq 4000 platform, generating ~25 million 76bp single-end reads per sample. Read quality trimming and adaptor removal was carried out using Trimmomatic (version 0.36) (25). The RSEM package (version 1.3.30) (26) in conjunction with the STAR alignment algorithm (version 2.5.2a) (27) was used for the mapping and subsequent gene-level counting of the sequenced reads with respect to Ensembl mouse GRCm.38.89 version transcriptome. All parameters were run as default except "–forward-prob" which was set to 0.5. Normalisation of raw count data and differential expression analysis was performed with the DESeq2 package (version 1.18.1) (28) within the R programming environment (version 3.4.3) (29). Differentially expressed genes were defined as those showing statistically significant differences (FDR <0.05) in the GSKi group relative to the Control Group for both Fibroblast and Macrophage datasets. To determine pathway and biological process enrichment, Clarivate Analytics's Metacore pathway analysis tools was used to determine pathway and biological process enrichment using a hypergeometric test. [https://portal.genego.com/]. Gene lists ranked by the Wald statistic were used to look for pathway and selected genesets using the Broad's GSEA software (version 2.1.0) with genesets from MSigDB (version 6) (30).

721 Differentially regulated genes (logFC > 1 and FDR < 0.05) from the fibroblast data
722 analysis were converted to human orthologs using HomoloGene
723 [https://www.ncbi.nlm.nih.gov/homologene]. Breast Carcinoma (BRCA) normalised
724 expression data was downloaded from the FireHose Broad GDAC website
725 [https://gdac.broadinstitute.org/] Data downloads were all version 2016012800.0.0.
726 BRCA patients were ranked using the sum of expression values of down regulated
727 gene signature. The top quartile of patients were names as "HIGH", and the bottom
728 quartile named "LOW". Survival plots were generated using R's survival package
729 (version 2.41-3) (31) and the level of statistical significance determined using the log
730 rank test.
731
732 *Animal procedures*

733 Mice used were: Wildtype mice in BALB/CJ background, MMTV-PyMT+, MMTV-
734 PyMT+ actin GFP mice and Rag1-/- in pure genetic FVB/N background and.
735 Animals were maintained under specific pathogen-free conditions and handled in
736 accordance with the Institutional Committees on Animal Welfare of the UK Home
737 Office and all the procedure were performed under the PPL P83B37B3C licence.
738
739 *Cell lines*

740 This study used a variety of breast cancer cell lines derived from the mouse normal
741 breast fibroblasts (mNBF) were a gift from E. Sahai and MMTV–PyMT cells were
742 isolated from MMTV–PyMT tumours (FVB/N background) as previously described (4).
743 The 4T1 and 4T07cell lines were provided by the Cell Services Unit of The Francis
744 Crick Institute.
745
746 4T1 cells plated in 2D were treated with either vehicle (DMSO) or 5 µM of
747 GSK269962A (Axon, 1167) for five days before performing in vitro and in vivo
748 experiments, unless stated differently. Media and inhibitors were changed daily.
749 Matrices of 2:1 Pure Collagen-I and Matrigel were prepared to a final collagen
750 concentration of ~4 mg/ml and a Matrigel concentration of ~2mg/ml. The cells were
751 seeded on top in 200ul of growth medium.
752
753 *Generation of shRNA plasmids*

754 The doxycycline inducible Tet-PLKO-puro lentiviral plasmid vector used in this study
755 was purchased from Addgene (#21915, #21916). The vector contains all the
756 necessary components for the controlled doxycycline-triggered expression of shRNA
757 in mammalian cells. Gene knock-down is triggered by the presence of doxycycline in
758 the growth media, while in the absence of doxycycline, shRNA expression is blocked
759 by the presence of constitutively-expressed TetR protein.
760 Forward and reverse oligonucleotides for a MYL9 and MYL12b-targeting shRNA and
761 a nontargeting shRNA construct were designed using The RNAi Consortium collection
762 (MISSION® shRNA, Sigma Aldrich).
763
764 *MACS isolation of cell subsets from tumour*

765

Tumour tissues were dissociated and processed to single-cells as described previously (4). MidiMACS separators and LD and LS columns (Milteny, 130-042-901, 130-042-401) were used to magnetically isolate mouse cellular subsets from tumour tissue at day 8 and day 14 and the procedure was performed on ice and promptly.

For fibroblast isolation, cells were isolated from Balb/cAnN mice orthotopically transplanted with 4T1 tumours pre-treated with DMSO or GSK. Single-cell suspensions were incubated with mouse FcR Blocking Reagent and subsequently with the following APC labelled antibodies – CD45, CD31, CD326 and hCD2. Cells were washed and incubated with magnetic anti-APC MicroBeads (Miltenyi, 130-090-855). Magnetically labelled immune, endothelial, epithelial and cancer cells were isolated using LD columns, washed thrice with 3 ml of MACS and the unlabelled flow-through cell fraction was the mesenchymal cells that we will refer to as fibroblasts hereafter. To increase the purity of the cells, the eluted fraction was applied to a second round of separation with a new LD column.

For macrophage isolation, F4/80+ cells were obtained by using the Anti-F4/80 MicroBeads UltraPure kit (Milteny, 130-110-443) following the manufacturer's instructions. Approximately $2x10^7$ single-cells from the tumour were stained with a mix of 180 µl MACS buffer and 20 µl of Anti-F4/80 MicroBeads for 15 minutes at 4°C in the dark. During this incubation, an LS column was placed onto a MidiMACS separator where magnetic field was applied, and the column was rinsed with 3 ml of MACS buffer. Cells were washed twice with 4 ml of MACS buffer and resuspended in 1ml prior to proceeding to magnetic separation by applying the cell suspension onto the column. Columns were washed thrice with 3 ml of MACS buffer before being carefully removed from the separator and placed on a FACS tube. 4.5 ml of MACS buffer was added onto the LS column and the plunger was firmly pushed to elute the F4/80+ cell fraction which had been retained within the column due to the F4/80+ positive selection. To increase the purity of the cells, the eluted fraction was applied to a second round of separation with a new LS column.

Alvetex scaffold 3D assay

Alvetex Scaffold 96-well plates (ReproCELL, AVP009) were washed once with 70% ethanol to render it hydrophilic. Following three washes with PBS, they were coated with a collagen-solution and incubated for 1 hour at 37°C prior to cell seeding. Primary MMTV–PyMT actin–GFP cells were seeded at a density of 5,000 cells per well and fibroblasts and macrophages isolated from tumours were seeded at a density of 25,000 cells per well in a total volume of 100ul of complete MMTV-PyMT media.
The growth of GFP+ cells was monitored every two days using the SteREO LumarV12 stereomicroscope (Zeiss) and for a total of 6 days. Images were taken at a magnification of 19.4X, Z +0.09, exposed for 2 seconds and quantified using ImageJ software. For quantification, images were stacked and the Li's minimum cross entropy thresholding algorithm was used. All data was normalized to the growth of PyMT-GFP cells at each timepoints.

Generation of conditioned media

100,000 4T1 cells (control or GSKi treated) were plated on tissue culture treated 24-well plates in 1 ml of complete DMEM media, which was conditioned at 37°C for 48 h. The medium preparation was collected and spun at 1200 rpm for 20 min. The supernatant after this centrifugation was collected and used as conditioned media (CM).

Fibroblast contraction assay

To assess fibroblast activation via their ability to remodel an extracellular matrix, $7{,}5x10_4$ mNBF cells were embedded in 100 µl of 2:1 collagen-I:Matrigel and seeded on a 35-mm glass-bottom dish (MatTek, P35-1.5-14-C). Once the gel had polymerized, a low height co-culture insert (Millipore, PICM-ORG-50) was placed on the dish and $1{,}5x10_5$ tumour cells were seeded on the insert in 1ml of complete DMEM media. Gel contraction was monitored daily by taking photographs of the gels. The gel contraction value refers to the contraction observed after 3 days, which was measured using ImageJ software and calculated as the gel area in arbitrary units (A.U.).

Cell proliferation assays – incucyte

Cells were plated sub-confluently with numbers ranging from 1,000 to 10,000 cells per well into 96-well high content imaging black plates (Corning, CLS4580). Cell growth was monitored over 4-6 days using IncuCyteZOOM® Live Cell Imaging. All conditions were performed in triplicate and 4 images per well were acquired every 3 hours. The total area covered by cells was automatically measured by the software through confluency masks. The percentage of confluency over time was calculated as the average area covered by cells relative to the total well area.

Cell migration assays

Chemotaxis of mNBF fibroblasts was assessed using Incucyte Clearview 96-well chemotaxis plate with ,2% pore density following the manufacturer's protocol (Essen Bioscience, 4582). 1,000 mNBF cells in DMEM with 1% FBS were loaded in the upper chamber compartment. CM from 4T1 DMSO or GSK was loaded in the lower chamber. Migration was monitored using the IncuCyteZOOM® Live Cell Imaging, and images of the upper and lower chambers were taken every hour. The total area covered by cells was automatically measured by image segmentation using the integrated chemotaxis analysis plugin.

Flow cytometry (FACS)

Prepared single-cell suspensions of mouse tissues and in vitro treated cancer cells were incubated with mouse FcR Blocking Reagent (Miltenyi, 130-092-575) for 10 min at 4°C followed by a 30 minute incubation at 4°C in the dark with a combination of the pre-labelled antibodies. Following two washes with MACS buffer, dead cells were stained with DAPI (4,6-Diamidino-2-phenylindole dihydrochloride, Sigma, D9542) and analysed with an LSRFortessa cell analyser running FACSDiva software (BD Biosciences) and FlowJo 10.4.2 software (FlowJO, LCC 2006-2018). All cell-sorting experiments were carried out using a BD Influx cell sorter (BD Biosciences).

857 *Antibodies*

858 Details of the primary antibodies used for immunohistochemistry in this study are listed
859 below.
860
861 Immunofluorescence

Antigen	Source Ig	Reactivity against	Dilution	Antigen retrieval	Catalogue number
SMA	Mouse	Mouse, Human	1:750	Citrate	DAKO, M0851
Endomucin	Rat	Mouse		Citrate	sc-65495
Collagen IV	Rabbit	Mouse	1:500	Citrate	USBiological C7510-50B
F4/80	Rat	Mouse	1:100	Trypsin	eBioscience, 14-4801
pSer19-MLC2	Rabbit polyclonal	Mouse, Human	1:50	Access super buffer	CST, 3671L

862
863 FACS

Antigen	Reacting Ig	Clone	Company	Dilution	Catalogue number
CD45-AF780	Mouse	30-F11	eBioscience	1:200	47-0451-82
CD45-bv421	Mouse	30-F11	Biolegend	1:200	103133
CD45-APC	Mouse	30-F11	eBioscience	1:200	17-0451-83
CD11b-AF780	Mouse	M1/70	eBioscience	1:100	47-0112-82
CD11b-APC	Mouse	M1/70	Biolegend	1:100	101212
F4/80-647	Mouse	BM8	eBioscience	1:100	MF48021
F4/80-AF780	Mouse	BM8	eBioscience	1:100	47-4801-82
CD31-PECy7	Mouse	390	eBioscience	1:100	25-0311-82
CD31-bv421	Mouse	390	Biolegend	1:100	102423
CD31-APC	Mouse	390	eBioscience	1:100	17-0311-82
hCD2-APC	Human	RPA-2.10	eBioscience	1:200	17-0029-42
CD19-bv421	Mouse	6D5	Biolegend	1:100	115549
CD11c-PE	Mouse	N418	eBioscience	1:100	12-0114-83
CD49f-PerCP-eFluor710	Mouse	ebioGOH3	eBioscience	1:100	46-0495-82
EPCAM-APC	Mouse	G8.8	eBioscience	1:100	17-5791-81
CD3e-AF780	Mouse	17A3	eBioscience	1:200	47-0032-80
Ly6G-bv450	Mouse	1A8	eBioscience	1:200	560603
Ly6G-PECy7	Mouse	1A8	Biolegend	1:100	127618
gd TCR-PECy7	Mouse	eBioGL3	eBioscience	1:100	25-5711-82
CD4-bv605	Mouse	GK1.5	Biolegend	1:100	100451
CD8-PE	Mouse	53-6.7	eBioscience	1:100	12-0081-82
CD163-PE	Mouse	TNKUPJ	Invitrogen	1:100	12-1631-82
MHCII-APC	Mouse	M5/114.15.2	Biolegend	1:100	107613
CD86-PECy7	Mouse	GL1	eBioscience	1:100	25-0862-82

CD206-647	Mouse		Life technologies	1:100	mca2235a647t
Arg1-PECy7	Mouse	A1exF5	Invitrogen	1:100	25-3697-82
iNOS-PE	Mouse	CXNFT	Invitrogen	1:100	12-5920-82

Refrences

1. Georgouli M, Herraiz C, Crosas-Molist E, Fanshawe B, Maiques O, Perdrix A, et al. Regional Activation of Myosin II in Cancer Cells Drives Tumor Progression via a Secretory Cross-Talk with the Immune Microenvironment. Cell. Elsevier Inc; 2019;176:757–774.e23.

2. Östman A, Augsten M. Cancer-associated fibroblasts and tumor growth--bystanders turning into key players. Current Opinion in Genetics & Development. 2009;19:67–73.

3. Sanz-Moreno V, Gaggioli C, Yeo M, Albrengues J, Wallberg F, Viros A, et al. ROCK and JAK1 Signaling Cooperate to Control Actomyosin Contractility in Tumor Cells and Stroma. Cancer Cell. Elsevier Inc; 2011;20:229–45.

4. Malanchi I, Santamaria-Martínez A, Susanto E, Peng H, Lehr H-A, Delaloye J-F, et al. Interactions between cancer stem cells and their niche govern metastatic colonization. Nature 2011;481:85–9.

5. Coussens LM, Werb Z. Inflammation and cancer. Nature. Nature Publishing Group; 2002;420:860–7.

6. Ogura M, Bridgeman VL, Malanchi I. Macrophages unlock progression of breast cancer cells experiencing matrigel-segregation in transplantation models. Sci Rep. Nature Publishing Group; 2017;7:1423.

7. Wculek SK, Malanchi I. Neutrophils support lung colonization of metastasis-initiating breast cancer cells. Nature. Nature Publishing Group; 2015;17:413–7.

8. Mantovani A, Marchesi F, Malesci A, Laghi L, Allavena P. Tumour-associated macrophages as treatment targets in oncology. Nat Rev Clin Oncol. 2017;144:2409.

9. Costa A, Kieffer Y, Scholer-Dahirel A, Pelon F, Bourachot B, Cardon M, et al. Fibroblast Heterogeneity and Immunosuppressive Environment in Human Breast Cancer. CCELL. Elsevier; 2018;33:463–479.e10.

10. Vicente-Manzanares M, Ma X, Adelstein RS, Horwitz AR. Non-muscle myosin II takes centre stage in cell adhesion and migration. Nat Rev Mol Cell Biol. Nature Publishing Group; 2009;10:778–90.

11. Rodriguez-Hernandez I, Cantelli G, Bruce F, Sanz-Moreno V. Rho, ROCK and actomyosin contractility in metastasis as drug targets. F1000Res. 2016;5:783.

12. Rodriguez-Hernandez I, Maiques O, Kohlhammer L, Cantelli G, Perdrix-Rosell A, Monger J, et al. WNT11-FZD7-DAAM1 signalling supports tumour initiating abilities and melanoma amoeboid invasion. Nature Communications. 11 ed. Springer US; 2020;11:1–20.

13. Kümper S, Mardakheh FK, McCarthy A, Yeo M, Stamp GW, Paul A, et al. Rho-associated kinase (ROCK) function is essential for cell cycle progression, senescence and tumorigenesis. Elife. eLife Sciences Publications, Ltd; 2016;5:e12994–4.

903 14. Wong P-P, Muñoz-Félix JM, Hijazi M, Kim H, Robinson SD, De Luxán-Delgado B, et al.
904 Cancer Burden Is Controlled by Mural Cell-β3-Integrin Regulated Crosstalk with Tumor Cells.
905 Cell. 2020;181:1346–1363.e21.

906 15. del Pozo Martin Y, Park D, Ramachandran A, Ombrato L, Calvo F, Chakravarty P, et al.
907 Mesenchymal Cancer Cell-Stroma Crosstalk Promotes Niche Activation, Epithelial Reversion,
908 and Metastatic Colonization. CellReports. The Authors; 2015;22:2456–69.

909 16. Orgaz JL, Crosas-Molist E, Sadok A, Perdrix-Rosell A, Maiques O, Rodriguez-Hernandez I,
910 et al. Myosin II Reactivation and Cytoskeletal Remodeling as a Hallmark and a Vulnerability in
911 Melanoma Therapy Resistance. CCELL. Elsevier Inc; 2020;37:85–9.

912 17. Wagner J, Rapsomaniki MA, Chevrier S, Anzeneder T, Langwieder C, Dykgers A, et al. A
913 Single-Cell Atlas of the Tumor and Immune Ecosystem of Human Breast Cancer. Cell.
914 2019;177:1330–1345.e18.

915 18. Friedman G, Levi-Galibov O, David E, Bornstein C, Giladi A, Dadiani M, et al. Cancer-
916 associated fibroblast compositions change with breast cancer progression linking the ratio of
917 S100A4 + and PDPN + CAFs to clinical outcome. Nature Cancer. Nature Publishing Group;
918 2020;1:692–708.

919 19. Noy R, Pollard JW. Tumor-associated macrophages: from mechanisms to therapy. Immunity.
920 2014;41:49–61.

921 20. Erez N, Truitt M, Olson P, Hanahan D. Cancer-Associated Fibroblasts Are Activated in
922 Incipient Neoplasia to Orchestrate Tumor-Promoting Inflammation in an NF-κB-
923 Dependent Manner. CCELL. Elsevier Ltd; 2010;17:135–47.

924 21. Albrengues J, Bourget I, Pons C, Butet V, Hofman P, Tartare-Deckert S, et al. LIF mediates
925 proinvasive activation of stromal fibroblasts in cancer. CellReports. 2014;7:1664–78.

926 22. Ombrato L, Nolan E, Kurelac I, Mavousian A, Bridgeman VL, Heinze I, et al. Metastatic-niche
927 labelling reveals parenchymal cells with stem features. Nature. Nature Publishing Group;
928 2019;572:603–8.

929 23. Van Rooijen N, Hendrikx E. Liposomes for specific depletion of macrophages from organs
930 and tissues. Methods Mol Biol. 2010;605:189–203.

931 24. Katlinski KV, Gui J, Katlinskaya YV, Ortiz A, Chakraborty R, Bhattacharya S, et al. Inactivation
932 of Interferon Receptor Promotes the Establishment of Immune Privileged Tumor
933 Microenvironment. CCELL. Elsevier Inc; 2017;31:194–207.

934 25. Bolger AM, Lohse M, Usadel B. Trimmomatic: a flexible trimmer for Illumina sequence data.
935 Bioinformatics. 2014;30:2114–20.

936 26. Li B, Dewey CN. RSEM: accurate transcript quantification from RNA-Seq data with or without
937 a reference genome. BMC Bioinformatics. BioMed Central; 2011;12:323.

938 27. Dobin A, Davis CA, Schlesinger F, Drenkow J, Zaleski C, Jha S, et al. STAR: ultrafast
939 universal RNA-seq aligner. Bioinformatics. 2012;29:15–21.

940 28. Love MI, Huber W, Anders S. Moderated estimation of fold change and dispersion for RNA-
941 seq data with DESeq2. Genome Biol. BioMed Central; 2014;15:550.

942 29. Team T. The R Project for Statistical Computing. wwwr-projectorg. 2008.

30. Subramanian A, Tamayo P, Mootha VK, Mukherjee S, Ebert BL, Gillette MA, et al. Gene set enrichment analysis: a knowledge-based approach for interpreting genome-wide expression profiles. Proc Natl Acad Sci USA. National Academy of Sciences; 2005;102:15545–50.

31. Therneau TM. Survival Analysis [R package survival version 3.2-3]. Comprehensive R Archive Network (CRAN); 2015. Available from: https://CRAN.R-project.org/package=survival